
LACK-OF-FIT REDUCTION IN THE PATH-INTEGRAL FORMALISM

Kateřina Mladá

Mathematical Institute, Faculty of Mathematics and Physics, Charles University,
Sokolovská 83, 18675 Prague, Czech Republic

Michal Pavelka

Mathematical Institute, Faculty of Mathematics and Physics, Charles University,
Sokolovská 83, 18675 Prague, Czech Republic
Corresponding author: pavelka@karlin.mff.cuni.cz

Václav Klika

Dept. of Mathematics, FNSPE, Czech Technical University in Prague,
Trojanova 13, 120 00 Prague, Czech Republic

June 26, 2025

ABSTRACT

We present a reformulation of the lack-of-fit reduction in non-equilibrium thermodynamics using the path-integral formalism. The reformulation is based on the Onsager-Machlup variational principle, and it allows us to minimize the action while keeping only thermodynamically relevant solutions. The reduced evolution consists of a Hamiltonian vector field and a gradient flow. The reformulation is illustrated on the Kac–Zwanzig model, where we show how irreversibility emerges from purely Hamiltonian evolution by ignoring some degrees of freedom. We also show how to generalize the Fisher information matrix and Kullback–Leibler divergence between two probability distributions to the case when the two distributions are related by the principle of maximum entropy, even in the case when the entropy is not of Boltzmann-Gibbs type (for instance Tsallis-Havrda-Charvát).

Contents

1	Introduction	2
2	GENERIC framework	4
3	A generalized Kullback–Leibler divergence	5
3.1	Classical Kullback–Leibler divergence	5
3.2	Principle of maximum entropy	6
3.3	A generalization of Kullback–Leibler divergence	6
3.4	Fisher information matrix	8
4	Thermodynamic paths minimizing an action	8
4.1	Exact solutions	9
4.2	Onsager-Machlup-like approximation	10

5	Lack-of-fit reduction	10
5.1	Path-integral formulation	11
5.2	Onsager-Machlup-like solution	14
5.3	Stochasticity	16
6	Kac–Zwanzig example	16
6.1	The Kac–Zwanzig model	17
6.2	Reduction by the Projection Operator Method	17
6.3	Lack-of-fit reduction	19
6.3.1	Formulation of the Lack-of-fit Lagrangian	19
6.3.2	The Hamilton–Jacobi equation	20
6.3.3	The reduced dynamics	21
6.3.4	Asymptotic solution of the Riccati equation	21
6.3.5	Stochasticity	23
6.3.6	Numerical results	24
6.3.7	KL Divergence	25
7	Conclusion	26
A	MaxEnt KL divergence with Tsallis-Havrda-Charvát entropy	27
B	Convexity of the dissipation potential	27
C	Details on the MaxEnt calculation	28
D	Details on solving the Hamilton–Jacobi equation	29
E	Alternative trajectories of the toy model	30
E.1	Quasistatic approximation	30
E.2	Steepest-descent approximation	30
E.3	Comparison of the approximate solutions	31
F	Calculation of the Kullback–Leibler divergence	33

1 Introduction

A purpose of non-equilibrium thermodynamics is to provide a framework for describing evolution of physical systems. For that purpose, it is necessary to have reduction methods, as any system can be described on various levels of description with different amounts of detail. In this paper, we use path integrals to measure the information discrepancy between a detailed and reduced description of a physical system, and by minimization of that discrepancy we obtain a set of reduced evolution equations.

The detailed evolution is assumed to be in the form of the General Equation for Non-Equilibrium Reversible-Irreversible Coupling (GENERIC), where the evolution is the sum of a reversible (Hamiltonian) part and irreversible (gradient) part Grmela and Öttinger (1997); Öttinger and Grmela (1997); Öttinger (2005); Pavelka et al. (2018). The reversible part is generated by a Poisson bracket and the Hamiltonian, while the irreversible part is generated by a dissipation potential and entropy. The reversible part is assumed to be purely mechanical, while the irreversible part is dissipative. In particular, the detailed evolution can be also purely Hamiltonian, while the reduced evolution will be always dissipative.

A general reduction method in non-equilibrium thermodynamics should satisfy the following criteria: (i) it should be compatible with the principle of maximum entropy, (ii) it should not require any fitting parameters, and (iii) it should be able to reduce a purely Hamiltonian system to a dissipative one. The lack-of-fit reduction Pavelka et al. (2020a); Mladá et al. (2024) satisfies all these criteria. The method is based on the Onsager-Machlup variational principle Onsager and Machlup (1953), and it minimizes the action while keeping only thermodynamically relevant solutions.

The lack-of-fit reduction Pavelka et al. (2020a) is based on the reduction method of Bruce Turkington and co-workers Turkington (2013), Turkington et al. (2016), Maack and Turkington (2018), Thalabard and Turkington (2017), where a variational principle was proposed that measures the discrepancy between the detailed and reduced dynamics. The method was further developed by Richard Kleeman Kleeman (2015), who added a path-integral formulation and a stochastic extension. In the current manuscript we reformulate the lack-of-fit reduction Pavelka et al. (2020a), that has already been tested on the Kac–Zwanzig model Mladá et al. (2024), by using the path-integral formulation of Kleeman (2015).

There are several other reduction methods in non-equilibrium thermodynamics. The Mori-Zwanzig projection operator method Mori (1965); Zwanzig (2001); Öttinger (2005) rewrites a second-order differential equation into an integro-differential first-order form with a memory kernel. The kernel is then approximated to obtain the reduced evolution Grabert (2006). Although this method often leads to a good approximation of the reduced evolution, characterized by a much larger time-scale than the detailed evolution, it often requires measurement of the fluctuations or fitting parameter Grabert (2006), and it now always leads to a dissipative term in the evolution.

The Ehrenfest reduction Gorban et al. (2001); Karlin et al. (2003); Pavelka et al. (2019) is another reduction method is based on an approximate dissipative solution of the detailed system. However, it requires a fitting parameter that expresses the relaxation time of the detailed dynamics towards the manifold of reduced variables Gorban and Karlin (2005). More recently, an interesting approach was proposed for coarse-graining of a dissipative Langevin equation Leadbetter et al. (2023), which shows remarkable robustness, and another approach was proposed based on finding a dissipative semigroup with an a priori known dissipation parameter Mielke et al. (2025).

To use the path-integral formulation for arbitrary concave entropy functionals, we generalize the Kullback–Leibler (KL) divergence and the Fisher information matrix to arbitrary entropies, using the principle of maximum entropy Kullback and Leibler (1951); Fisher and Russell (1922); Jaynes (1967). Finally, we obtain a simpler version of the lack-of-fit

reduction than before Pavelka et al. (2020a), and we test it on the Kac–Zwanzig model, including the stochastic version of the reduced dynamics.

In Section 2, we recall the GENERIC framework, Section 3 is devoted to the generalized KL divergence and the Fisher information matrix, and Section 4 illustrates how to minimize the action while keeping only thermodynamically relevant solutions. In Section 5, we present the lack-of-fit reduction in the path-integral formalism. Finally, in Section 6, we apply the method to the Kac–Zwanzig model, and we show how different choices of the reduced state variables agree with the detailed numerical simulations, based on their KL divergence with respect to the distribution of the detailed state variables.

2 GENERIC framework

Within the GENERIC framework Grmela and Öttinger (1997); Öttinger and Grmela (1997); Öttinger (2005); Pavelka et al. (2018), evolution of any set of state variables \mathbf{x} is the sum of two contributions, one of which is Hamiltonian and the other one is dissipative,

$$\dot{\mathbf{x}} = \uparrow\{\mathbf{x}, \uparrow E\} + \left. \frac{\delta \uparrow \Xi}{\delta \mathbf{x}^*} \right|_{\mathbf{x}^* = \frac{\delta \uparrow S}{\delta \mathbf{x}}} \quad (1)$$

The Hamiltonian (reversible) evolution is generated by a Poisson bracket $\{, \}$ and the Hamiltonian E (the energy). The dissipative part is generated by a dissipation potential $\uparrow \Xi$ and entropy $\uparrow S$ (the conjugate variables \mathbf{x}^* are obtained from the entropy $\uparrow S(\mathbf{x})$ by the functional derivative). The Poisson bracket is bilinear, skew-symmetric, and it satisfies the Leibniz rule and the Jacobi identity. Skew-symmetry ensures that the energy is conserved by the Hamiltonian evolution. The Leibniz rule makes the bracket work like a derivative, so the evolution equations are invariant with respect to adding constants to the energy. Before explaining the Jacobi identity, we shall first recall the concept of Poisson bivector.

The GENERIC evolution can be also seen as being generated by a vector field \mathbf{X} , components of which have the form

$$X^i = \uparrow L^{ij} \frac{\partial \uparrow E}{\partial x^j} + \left. \frac{\partial \uparrow \Xi}{\partial x_i^*} \right|_{\mathbf{x}^* = \frac{\delta \uparrow S}{\delta \mathbf{x}}} \quad (2)$$

where

$$\uparrow L^{ij} = \uparrow \{x^i, x^j\} \quad (3)$$

are the components of a Poisson bivector (actually a twice contravariant tensor field). The Jacobi identity can be then interpreted as that the Lie derivative of the bivector with respect to the Hamiltonian part of the vector field is zero Fecko (2006); Pavelka et al. (2020b).

The dissipation potential $\uparrow \Xi$ depends on the conjugate variables so that it has a minimum at $\mathbf{x}^* = 0$, and it is convex near that point. It should not change the overall energy of the system, for which a degeneracy condition is needed Kraaij et al. (2018). Moreover, it can also depend directly on the state variables \mathbf{x} , which is needed for instance in the case of chemical reactions Grmela (2012); Mielke et al. (2014). The dissipation potential generates a gradient flow, which can

be also seen as the most probable path of a stochastic system obeying a large-deviation principle Mielke et al. (2014); Kraaij et al. (2018); Öttinger et al. (2021); Montefusco et al. (2021).

When we have a reduced set of state variables \mathbf{y} obtained by a projection $\pi : \mathbf{x} \rightarrow \mathbf{y}$, the Poisson bivector can be projected onto the reduced state space as

$$\downarrow L^{ab} = \uparrow \{y^a, y^b\} = \frac{\partial y^a}{\partial x^i} \frac{\partial y^b}{\partial x^j} (\uparrow L^{ij}). \quad (4)$$

If the resulting $\downarrow L^{ab}$ is independent of \mathbf{x} , the corresponding bracket satisfies the Jacobi identity. In other cases, another mapping $\mathbf{x}(\mathbf{y})$ might be necessary to remove that dependence, and it is often the maximum entropy mapping, discussed in the following Section.

The reduced evolution can also be expressed in a dual form, where conjugate variables \mathbf{y}^* are obtained as Legendre transformations of \mathbf{y} , and the Poisson bivector then transforms as a twice contravariant tensor field,

$$\downarrow L_{ab}^* = \uparrow \{y_a^*, y_b^*\} |_{\mathbf{x}(\mathbf{y}^*)} = \frac{\partial y_a^*}{\partial x^i} \frac{\partial y_b^*}{\partial x^j} (\uparrow L^{ij}) |_{\mathbf{x}(\mathbf{y}^*)}. \quad (5)$$

These forms of the Poisson bivector will help us later when deriving the reduced evolution equations by means of the lack-of-fit reduction.

A similar structure as GENERIC can be found in Dzyaloshinskii and Volovick (1980); Beris and Edwards (1994), where entropy density is among the state variables. When the dissipation potential is quadratic, its Hessian plays the role of a metric, and the evolution equations then obtain the metriplectic form Morrison (1984); Grmela (1984), where dissipative part of a can be also expressed using a dissipative bracket Öttinger (2005), which in some generalizations even turns out not fully symmetric Öttinger (2005). After a short review of the GENERIC framework, let us now recall the concept of Kullback–Leibler divergence, which will be used in the lack-of-fit reduction.

3 A generalized Kullback–Leibler divergence

Before formulating the lack-of-fit reduction, we have to recall the concept of Kullback–Leibler divergence, and we have to generalize it so that we can work with an arbitrary concave entropy $\uparrow S$.

3.1 Classical Kullback–Leibler divergence

The Kullback–Leibler (KL) divergence is a measure of the difference between two probability distributions Kullback and Leibler (1951). It is defined as

$$D_{KL}(\mathbf{p}||\mathbf{q}) = \sum_i p_i \ln \frac{p_i}{q_i} \quad (6)$$

where \mathbf{p} and \mathbf{q} are two probability distributions. The KL divergence is non-negative, as can be proved by noting that $\ln(x) \leq x - 1$, and is equal to zero if and only if the two distributions are identical.

The form of KL divergence is strongly tied with the Shannon entropy Shannon (1948). What if the distributions are connected with another entropy, for instance by means of the principle of maximum entropy (MaxEnt) Jaynes (1967); Pavelka et al. (2018)? Let us now generalize the KL divergence to the case when the two distribution are related by MaxEnt.

3.2 Principle of maximum entropy

Let us first recall the geometric formulation of MaxEnt Grmela et al. (2015). Assume that a detailed set of state variables \mathbf{x} is equipped with entropy $\uparrow S(\mathbf{x})$, which is a function of the state variables. A reduced set of state variables \mathbf{y} is obtained by a projection $\pi : \mathbf{x} \rightarrow \mathbf{y}$. The MaxEnt estimate of \mathbf{x} based on the knowledge of \mathbf{y} is obtained in two steps.

First, the MaxEnt estimate is calculated as a function of the reduced conjugate variables \mathbf{y}^* by

$$\frac{\partial}{\partial \mathbf{x}} (-\uparrow S(\mathbf{x}) + y_a^* \pi^a(\mathbf{x})) = 0, \quad (7)$$

or

$$\left. \frac{\partial \uparrow S}{\partial x^i} \right|_{\mathbf{x}(\mathbf{y}^*)} = \left. \frac{\partial \pi^a}{\partial x^i} \right|_{\mathbf{x}(\mathbf{y}^*)} y_a^*, \quad (8)$$

which determines the MaxEnt dependence $\mu : \mathbf{y} \rightarrow \mathbf{x}(\mathbf{y}^*)$. This also defines the reduced conjugate entropy

$$\downarrow S^*(\mathbf{y}^*) = -\uparrow S(\mathbf{x}(\mathbf{y}^*)) + y_a^* \pi^a(\mathbf{x}(\mathbf{y}^*)). \quad (9)$$

Second, the Legendre transform converts the reduced conjugate variables \mathbf{y}^* to the reduced state variables \mathbf{y} by solving

$$\frac{\partial}{\partial \mathbf{y}^*} (-\uparrow S^*(\mathbf{y}^*) + y_a y_a^*) = 0, \quad (10)$$

which gives the mapping $\mathbf{y}^*(\mathbf{y})$ as well as the reduced entropy

$$\downarrow S(\mathbf{y}) = -\downarrow S^*(\mathbf{y}^*(\mathbf{y})) + y_a y_a^*(\mathbf{y}). \quad (11)$$

Altogether, the MaxEnt procedure gives the mappings $\mathbf{x}(\mathbf{y}^*)$, $\mathbf{y}^*(\mathbf{y})$, the reduced conjugate entropy $\downarrow S^*(\mathbf{y}^*)$, and the reduced entropy $\downarrow S(\mathbf{y})$. Note that the reduced entropy can also be obtained by inserting the mapping $\mathbf{x}(\mathbf{y}^*(\mathbf{y}))$ into the original entropy $\uparrow S(\mathbf{x})$. Several other useful formulas can be found in Appendix C.

3.3 A generalization of Kullback–Leibler divergence

Assume now that the second distribution in the KL divergence is obtained from the first one by the MaxEnt procedure and that the entropy $\uparrow S(\mathbf{p})$ is of the Shannon (or Boltzmann-Gibbs) type,

$$\uparrow S(\mathbf{p}) = -k_B \sum_i p_i \ln(\alpha p_i), \quad (12)$$

where α is a constant (typically equal to the unity for discrete distribution and to a power of the Planck constant for distribution on a phase space). The distribution \mathbf{p} plays the role of the detailed state variables here. The reduced variables \mathbf{y} are obtained as averages of the distribution \mathbf{p} , $y^a = \sum_i \pi_i^a p_i$.

The MaxEnt estimate of the distribution \mathbf{p} subject to knowledge of the reduced variables is again obtained in two steps. First, the MaxEnt estimate is calculated as a function of the reduced conjugate variables \mathbf{y}^* as

$$\frac{\partial}{\partial \mathbf{p}} (-\uparrow S(\mathbf{p}) + y_a^* \pi^a(\mathbf{p})) = 0 \quad \Rightarrow \quad p_i(\mathbf{y}^*) = \frac{1}{\alpha} e^{-y_a^* \pi_i^a / k_B - 1} \stackrel{def}{=} q_i. \quad (13)$$

When this estimate is used as the second distribution in the KL divergence, we obtain

$$D_{KL}(\mathbf{p}||\mathbf{q}) = \sum_i p_i \ln \frac{p_i}{q_i} = \frac{1}{k_B} \underbrace{(-\uparrow S(\mathbf{p}) + y_a^* \pi^a(\mathbf{p}))}_{\stackrel{def}{=} \downarrow \tilde{S}(\mathbf{p}, \mathbf{y}^*)} + \nu \quad (14)$$

where $\nu = \sum_i p_i$ is the normalization constant (typically $\nu = 1$). The first term in the expression for the KL divergence is the reduced conjugate entropy before the detailed variable is evaluated at the MaxEnt estimate, and we shall refer to this as the reducing potential $\downarrow \tilde{S}^*(\mathbf{x}, \mathbf{y}^*)$ Grmela (2024).

The normalization constant is related to the reduced conjugate entropy,

$$\downarrow S^*(\mathbf{y}^*) = -k_B \nu. \quad (15)$$

The KL divergence can then be expressed as the MaxEnt Kullback–Leibler divergence $D_{KL}^M(\mathbf{x}||\mathbf{y}) \stackrel{def}{=} D_{KL}^{M*}(\mathbf{x}||\mathbf{y}^*)|_{\mathbf{y}^*(\mathbf{y})}$, where the conjugate MaxEnt KL divergence is defined as

$$D_{KL}^{M*}(\mathbf{x}||\mathbf{y}^*) = \frac{1}{k_B} \left(\downarrow \tilde{S}^*(\mathbf{x}, \mathbf{y}^*) - \downarrow S^*(\mathbf{y}^*) \right). \quad (16)$$

The MaxEnt KL-divergence $D_{KL}^M(\mathbf{x}||\mathbf{y}) \stackrel{def}{=} D_{KL}^{M*}(\mathbf{x}||\mathbf{y}^*(\mathbf{y}))$ is obtained by evaluating the conjugate divergence at \mathbf{y} that corresponds to \mathbf{y}^* by Legendre transformation of $\downarrow S^*$. This generalized KL divergence is automatically non-negative as $\downarrow \tilde{S}^*(\mathbf{x}, \mathbf{y}^*) \geq \downarrow S^*(\mathbf{y}^*)$, and it can be seen as a generalization of the usual KL divergence because it does not rely on the Shannon form of the entropy.

The generalized MaxEnt KL divergence simplifies to the usual KL divergence in the case of Shannon entropy when \mathbf{x} is a probability distribution with probabilities p_i and \mathbf{y} a distribution with probabilities q_i . In Appendix A, we show how the generalized MaxEnt KL divergence works in the case of Tsallis-Havrda-Charvát entropy Tsallis (1988); Havrda and Charvát (1967); Jizba and Korbel (2019).

3.4 Fisher information matrix

The Fisher information matrix Fisher and Russell (1922); Rao (1992) is a measure of the amount of information that an observable random variable \mathbf{p} carries about an unknown parameter \mathbf{y} ,

$$I_{ab}(\mathbf{p}, \mathbf{y}) = \sum_i \frac{\partial \ln p_i}{\partial y^a} \frac{\partial \ln p_i}{\partial y^b} p_i = - \sum_i \frac{\partial^2 \ln p_i}{\partial y^a \partial y^b} p_i, \quad (17)$$

and it can be seen as the Hessian of the KL divergence with respect to the parameters \mathbf{y} .

Similarly, the MaxEnt Fisher information matrix can be defined as the pullback of the Hessian with respect to the detailed variables \mathbf{x} ,

$$I_{ab}^M(\mathbf{y}) = -\mu^* (d^{2\uparrow} S)_{ab} = - \left. \frac{\partial x^i}{\partial y^a} \frac{\partial^2 \uparrow S}{\partial x^i \partial x^j} \right|_{\mathbf{x}(\mathbf{y})} \frac{\partial x^j}{\partial y^b} \quad (18)$$

because

$$\downarrow \tilde{S}^*(\mathbf{x}(\mathbf{y}^*) + d\mathbf{x}, \mathbf{y}^*) = \downarrow S^*(\mathbf{y}^*) - \underbrace{\frac{\partial \uparrow S}{\partial x^i} \Big|_{\mathbf{x}(\mathbf{y}^*)}}_{=0} + y_a^* \pi_i^a x^i(\mathbf{y}^*) - \frac{1}{2} \underbrace{\frac{\partial^2 \uparrow S}{\partial x^i \partial x^j} \Big|_{\mathbf{x}(\mathbf{y}^*)}}_{d^{2\uparrow} S} dx^i dx^j + \mathcal{O}(dx^3). \quad (19)$$

In the case of Shannon entropy $\uparrow S(\mathbf{p})$, the MaxEnt Fisher information matrix coincides with the standard Fisher information matrix (17). The MaxEnt Fisher information matrix (18) is a generalization of the standard Fisher information matrix (17) because it does not rely on the Shannon form of the entropy.

The MaxEnt Fisher information matrix can be also expressed in terms of the conjugate variables \mathbf{y}^* as

$$I_{ab}^{M*}(\mathbf{y}^*) = - \left. \frac{\partial x^i}{\partial y_a^*} \frac{\partial^2 \uparrow S}{\partial x^i \partial x^j} \right|_{\mathbf{x}(\mathbf{y}^*)} \frac{\partial x^j}{\partial y_b^*}, \quad (20)$$

which will be useful later in this manuscript.

4 Thermodynamic paths minimizing an action

The purpose of this section is to illustrate on a simple toy example how to minimize the action while keeping only some solutions that are thermodynamically relevant. Motivated by Kleeman (2015), we consider the Lagrangian

$$2\mathcal{L} = \dot{u}^2 + \kappa^2 u^2, \quad (21)$$

where $u(t)$ is a function of time and κ is a positive constant. If we replaced the plus sign in the Lagrangian with a minus sign, we would get the Lagrangian of a harmonic oscillator. Lagrangian (21) describes a system with a potential that may grow with time and such solutions would not be thermodynamically relevant. Therefore, we shall study stationary points of the action

$$S = \int_0^T \mathcal{L} dt = \int_0^T \frac{(\dot{u}^2 + \kappa^2 u^2)}{2} dt, \quad (22)$$

where T is the time of the evolution, while looking for particular extremes that lead to equilibrium solutions. The action is a function of the initial and final values of $u(t)$, $u_0 = u(0)$ and $u_T = u(T)$, and the time T , and we keep the initial value and time fixed while possibly letting the end value and time vary.

4.1 Exact solutions

All geodesics, or stationary points of action (22), must solve the Euler–Lagrange equation

$$\ddot{u} = \kappa^2 u. \quad (23)$$

The solutions (geodesics) are given by the initial and final values u_0, u_T ,

$$u(t) = Ae^{\kappa t} + Be^{-\kappa t}, \quad A = u_0 - B, \quad B = \frac{1}{2} \frac{u_0 e^{\kappa T} - u_T}{\sinh \kappa T}, \quad (24)$$

and they consist of a damped exponential as well as exponential blow-ups.

The action itself evaluated at the geodesics becomes

$$S_e = \frac{\kappa}{2} \left[\coth(\kappa T) (u_0^2 + u_T^2) - \frac{2u_0 u_T}{\sinh(\kappa T)} \right]. \quad (25)$$

and is plotted in Figure 1. As we eventually strive for thermodynamically relevant solutions only, where the action

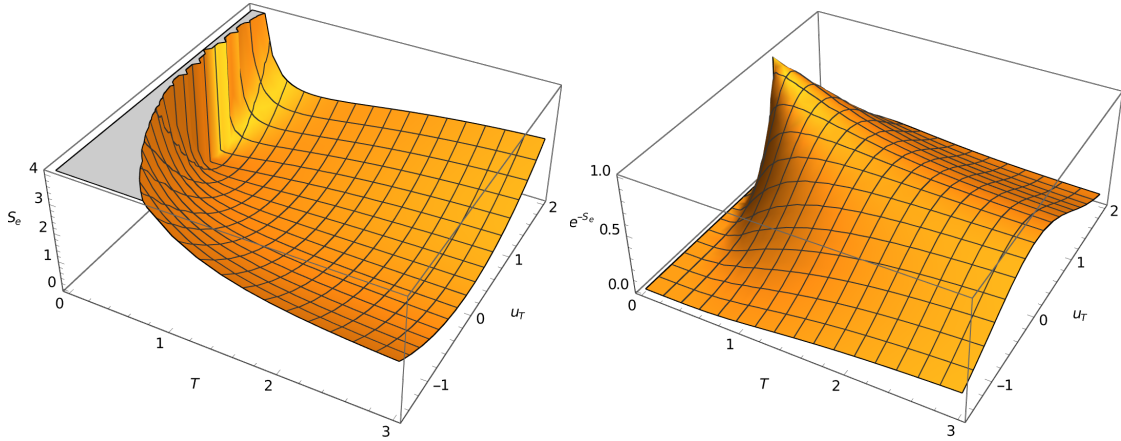


Figure 1: Extremal action $S_e(T, u_T)$ (25) and the "distribution" $\exp(-S_e(T, u_T))$. The initial value is taken as $u_0 = 1$ and $\kappa = 1$.

represents the Kullback–Leibler divergence, we need to eliminate the exponentially growing parts of the geodesics. Before doing so, we shall recall how the action can be sought in a different way, namely by using the Hamilton–Jacobi equation.

When the final time and value of u are free, the action evaluated at the geodesics satisfies the Hamilton–Jacobi equation Gelfand and Fomin (2012)

$$\frac{\partial S}{\partial t} + \frac{1}{2} \left[\left(\frac{\partial S}{\partial u} \right)^2 - \kappa^2 u^2 \right] = 0. \quad (26)$$

This equation is solved in D and the solution is the same as the one obtained from the Euler–Lagrange equation (25). The equation, however, still contains exponentially growing parts. In the following section, we will show how to eliminate them and obtain a solution that is thermodynamically relevant.

4.2 Onsager-Machlup-like approximation

One possible approach, that will be used in the general theory, is the Onsager-Machlup-like (OM) approximation. The idea is to rewrite the Lagrangian (21) in the form of a square plus a function of time only,

$$\mathcal{L} = \frac{1}{2} (\dot{u}^2 + \kappa^2 u^2) = \frac{1}{2} (\dot{u} + \kappa u)^2 - \frac{d}{dt} \left(\kappa \frac{u^2}{2} \right), \quad (27)$$

which leads to the action

$$S = \int_0^T \frac{1}{2} (\dot{u} + \kappa u)^2 dt - \frac{1}{2} \kappa (u_T^2 - u_0^2). \quad (28)$$

When the initial and final values are fixed, the action is minimized when the first term disappears, that is when the geodesics satisfy the equation

$$\dot{u} + \kappa u = 0 \implies u(t) = u_0 e^{-\kappa t}. \quad (29)$$

Other approximate solutions are discussed in E.

When we only choose those geodesics corresponding to the minimum of the action, we discard all geodesics that are stationary points of the action but not minima. This effectively means that we reduce the order of the differential equation describing geodesics to an equation of first degree in time, instead of the second-degree Euler–Lagrange equation.

In the following section, we shall use the OM approximate solution in a general theory of non-equilibrium thermodynamic reduction.

5 Lack-of-fit reduction

In this section, we provide a variant of the lack-of-fit reduction in non-equilibrium thermodynamics that is based on the Onsager-Machlup path-integral formalism Onsager and Machlup (1953), generalizing works of Bruce Turkington Turkington (2013); Turkington et al. (2016); Maack and Turkington (2018); Thalabard and Turkington (2017), Richard Kleeman Kleeman (2015), and ours Pavelka et al. (2020a); Mladá et al. (2024).

The lack-of-fit method reduces a detailed description of a physical system to a less detailed description by taking into account only some degrees of freedom. The basic idea is to minimize the discrepancy (lack of fit) between the detailed and reduced evolution equations near the MaxEnt submanifold (the image of the MaxEnt mapping from the reduced state space to the detailed space). The reduced dynamics then contains dissipative terms that are derived from the detailed evolution. In particular, even purely Hamiltonian systems can be reduced to a dissipative dynamics, and the

method does not require any fitting parameters. In the present manuscript, we formulate the lack-of-fit reduction in the context of the path-integral formalism Kleeman (2015).

5.1 Path-integral formulation

The path-integral formalism builds upon the Onsager-Machlup (OM) variational principle Onsager and Machlup (1953). The principle is formulated as a Wiener path integral with the path amplitudes W

$$W[\mathbf{y}^*(t)] = C \exp \left[-\frac{\Delta t}{k_B} \int_0^t dt \mathcal{L}(\mathbf{y}^*, \dot{\mathbf{y}}^*) \right], \quad (30)$$

where Δt is a characteristic time-scale, k_B is the Boltzmann constant, $\mathbf{y}^*(t)$ is a path of some chosen variables, $\mathcal{L}(\mathbf{y}^*, \dot{\mathbf{y}}^*)$ is a Lagrangian, and C is a normalization constant. In the OM near-equilibrium case, $\mathcal{L}(\mathbf{y}^*, \dot{\mathbf{y}}^*) = (\dot{\mathbf{y}}^* - \mathbf{U}\mathbf{y}^*)^T \mathbf{g}(\dot{\mathbf{y}}^* - \mathbf{U}\mathbf{y}^*)$, with \mathbf{g} and \mathbf{U} being constant matrices. The probability $p(\mathbf{y}^*, T)$ as a function of the variable \mathbf{y}^* at a particular time T is Kleeman (2015)

$$p(\mathbf{y}_T^*, T) = C \int d\mathbf{y}_0^* p(\mathbf{y}_0^*) K(\mathbf{y}_0^*, \mathbf{y}_T^*), \quad (31)$$

with the kernel

$$K(\mathbf{y}_0^*, \mathbf{y}_T^*) = C \int_{\mathbf{y}^*(0)=\mathbf{y}_0^*, \mathbf{y}^*(T)=\mathbf{y}_T^*} W[\mathbf{y}^*(t)] \mathcal{D}\mathbf{y}^*. \quad (32)$$

The most probable path is then obtained by minimizing the action $\int_0^T \mathcal{L}(\mathbf{y}^*, \dot{\mathbf{y}}^*) dt$ as $\dot{\mathbf{y}}^* = \mathbf{U}\mathbf{y}^*$, similarly as in the approximate solution obtained in Section 4.

Suppose now that some detailed variables \mathbf{x} are reduced to a set of reduced variables \mathbf{y} by a projection $\pi : \mathbf{x} \rightarrow \mathbf{y}$. If one knows only the reduced variables, the most probable values of the detailed variables can be expressed as functions of the reduced variables (or their conjugates) as the MaxEnt mapping $\mathbf{x}(\mathbf{y}^*)$. We assume that the detailed system is such that it stays close to the MaxEnt submanifold, and if it deviates from the submanifold, it falls back within a typical time $(\Delta t)_y$, as in Gorban and Karlin (2005). The information discrepancy between the detailed path $\mathbf{x}(t)$ and reduced path $\mathbf{y}^*(t)$ can be then measured as the MaxEnt Kullback–Leibler divergence between the detailed and reduced variables, summed over points ($i = 1, \dots, N$) along the path,

$$\begin{aligned} \Delta_{\text{lack of fit}} &= \sum_i D_{KL}^{M*}(\mathbf{x}(t_i) || \mathbf{y}^*(t_i)) = \frac{1}{(\Delta t)_y} \sum_i D_{KL}^{M*}(\mathbf{x}(t_i) || \mathbf{y}^*(t_i)) (\Delta t)_y \\ &\approx \frac{1}{(\Delta t)_y} \int_0^T D_{KL}^{M*}(\mathbf{x}(t) || \mathbf{y}^*(t)) dt. \end{aligned} \quad (33)$$

The factor $(\Delta t)_y$ is the time-scale of the reduced variables, which is typically much larger than the time-scale of the detailed variables $(\Delta t)_x$.

Let us now simplify the information discrepancy by expanding the MaxEnt KL divergence in the detailed variables. Equation (19) tells that

$$D_{KL}^{M*}(\mathbf{x} + \delta\mathbf{x}||\mathbf{y}^*) \approx -\frac{1}{2k_B} \delta x^i \left. \frac{\partial^2 \uparrow S}{\partial x^i \partial x^j} \right|_{\mathbf{x}(\mathbf{y}^*)} \delta x^j, \quad (34)$$

where $\delta\mathbf{x}$ is the difference between the exact evolution of \mathbf{x} and the MaxEnt estimate of the evolution.

More precisely, when the system is in state $\mathbf{x}(\mathbf{y}^*)$ at time t , then at a slightly later time $t + (\Delta t)_x$, the detailed evolution is at $\mathbf{x}_1 = \mathbf{x}(\mathbf{y}^*) + \Delta\mathbf{x}$. The MaxEnt image $\mathbf{x}(\mathbf{y}^*)$, which evolves with the reduced variables, is at $\mathbf{x}_2 = \mathbf{x}(\mathbf{y}^*) + (\Delta\mathbf{x})_y$, where $(\Delta\mathbf{x})_y \approx \frac{\partial \mathbf{x}}{\partial \mathbf{y}^*} \Delta\mathbf{y}^*$. The expansion of the MaxEnt KL divergence with $\delta\mathbf{x} = \mathbf{x}_2 - \mathbf{x}_1$ can be then expressed as

$$\begin{aligned} D_{KL}^{M*}(\mathbf{x}||\mathbf{y}^*) &\approx -\frac{1}{2k_B} (x_2^i - x_1^i) \left. \frac{\partial^2 \uparrow S}{\partial x^i \partial x^j} \right|_{\mathbf{x}(\mathbf{y}^*)} (x_2^j - x_1^j) \\ &= -\frac{1}{2k_B} (\Delta x^i - (\Delta x^i)_y) \left. \frac{\partial^2 \uparrow S}{\partial x^i \partial x^j} \right|_{\mathbf{x}(\mathbf{y}^*)} (\Delta x^j - (\Delta x^j)_y) \\ &= -\frac{(\Delta t)_x^2}{2k_B} \left(\frac{\Delta x^i}{(\Delta t)_x} - \frac{(\Delta x^i)_y}{(\Delta t)_x} \right) \left. \frac{\partial^2 \uparrow S}{\partial x^i \partial x^j} \right|_{\mathbf{x}(\mathbf{y}^*)} \left(\frac{\Delta x^j}{(\Delta t)_x} - \frac{(\Delta x^j)_y}{(\Delta t)_x} \right). \end{aligned} \quad (35)$$

The information discrepancy (33) can then be approximated as

$$\begin{aligned} \Delta_{\text{lack of fit}} &\approx -\frac{1}{2k_B} \frac{(\Delta t)_x^2}{(\Delta t)_y} \int_0^T dt \left(\frac{\Delta x^i}{(\Delta t)_x} - \frac{(\Delta x^i)_y}{(\Delta t)_x} \right) \left. \frac{\partial^2 \uparrow S}{\partial x^i \partial x^j} \right|_{\mathbf{x}(\mathbf{y}^*)} \left(\frac{\Delta x^j}{(\Delta t)_x} - \frac{(\Delta x^j)_y}{(\Delta t)_x} \right) \\ &\approx -\frac{\Delta t}{2k_B} \int_0^T dt \left(\dot{\mathbf{x}}^i - \frac{\partial \mathbf{x}^i}{\partial \mathbf{y}_a^*} \dot{\mathbf{y}}_a^* \right) \left. \frac{\partial^2 \uparrow S}{\partial x^i \partial x^j} \right|_{\mathbf{x}(\mathbf{y}^*)} \left(\dot{\mathbf{x}}^j - \frac{\partial \mathbf{x}^j}{\partial \mathbf{y}_b^*} \dot{\mathbf{y}}_b^* \right), \end{aligned} \quad (36)$$

where the time pre-factor is defined as the ratio of the short and slow time-scales multiplied by the short time-scale, that is $\Delta t = \frac{(\Delta t)_x^2}{(\Delta t)_y}$. Figure 2 illustrates the construction of the variational lack-of-fit discrepancy.

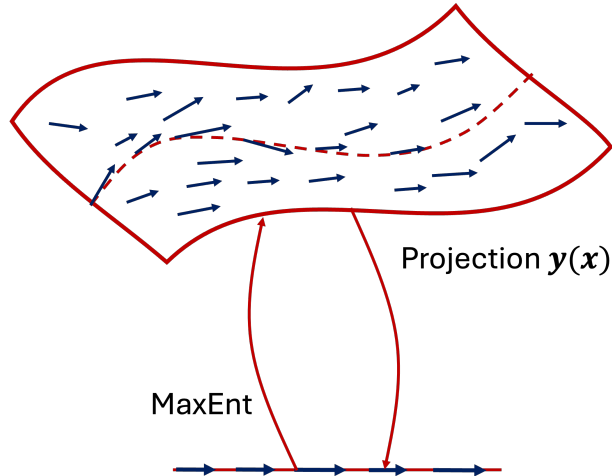


Figure 2: The lack-of-fit discrepancy is measured as the difference between the detailed vector field $\dot{\mathbf{x}}$ in the vicinity of the MaxEnt submanifold and the MaxEnt image of the reduced vector field $\dot{\mathbf{y}}^*$.

The path integral then becomes dependent on the reduced conjugate variables,

$$K(\mathbf{y}_0^*, \mathbf{y}_T^*) = \int_{\mathbf{y}^*(0)=\mathbf{y}_0^*, \mathbf{y}^*(T)=\mathbf{y}_T^*} C \exp \left(-\frac{\Delta t}{k_B} \int_0^T dt \mathcal{L}(\mathbf{y}^*, \dot{\mathbf{y}}^*) \right) \mathcal{D}\mathbf{y}^*, \quad (37)$$

with Lagrangian

$$\mathcal{L}(\mathbf{y}^*, \dot{\mathbf{y}}^*) = -\frac{1}{2} \left(R^i \frac{\partial^2(\uparrow S)}{\partial x^i \partial x^j} \Big|_{\mathbf{x}(\mathbf{y}^*)} R^j \right), \quad (38)$$

where the residuum R^i is

$$R^i(\mathbf{x}(\mathbf{y}^*)) = \uparrow L^{ij}(\mathbf{x}(\mathbf{y}^*)) \frac{\partial \uparrow \bar{E}}{\partial x^j} + \frac{\partial \uparrow \Xi}{\partial x_i^*} \Big|_{\mathbf{x}^* = \frac{\partial \uparrow S}{\partial \mathbf{x}}} - \frac{\partial x^i}{\partial y_a^*} \dot{y}_a^*, \quad (39)$$

similarly as in Pavelka et al. (2020a); Mladá et al. (2024). The residuum expresses the difference between the vector field on the MaxEnt submanifold and the image of the reduced vector field obtained by the MaxEnt mapping. The apparent detailed energy $\uparrow \bar{E}(\mathbf{x}) = \downarrow E(\mathbf{y}(\mathbf{x}))$, which is present in the residuum, is defined as the projection pullback of the reduced energy

$$\downarrow E(\mathbf{y}) \stackrel{def}{=} E(\mathbf{x}(\mathbf{y})). \quad (40)$$

The detailed evolution vector field \mathbf{X} is assumed to be of the GENERIC form (2). In particular, it can be purely Hamiltonian without any dissipation potential.

The most probable path $\mathbf{y}^*(t)$ is then obtained by minimizing the action

$$\Delta \Sigma[\mathbf{y}^*(t)] \equiv \int_0^T \mathcal{L}(\mathbf{y}^*, \dot{\mathbf{y}}^*) dt. \quad (41)$$

Since the Lagrangian (38) is quadratic in $\dot{\mathbf{y}}^*$, we may write \mathcal{L} in the form (following the notation from Kleeman (2015))

$$\mathcal{L} = \frac{1}{2} \dot{\mathbf{y}}^{*T} g \dot{\mathbf{y}}^* - \dot{\mathbf{y}}^* \downarrow \mathbf{X} + \frac{1}{2} \|\mathbf{X}\|^2, \quad (42)$$

where

$$g^{ab} = -\frac{\partial x^i}{\partial y_a^*} \frac{\partial^2(\uparrow S)}{\partial x^i \partial x^j} \Big|_{\mathbf{x}(\mathbf{y}^*)} \frac{\partial x^j}{\partial y_b^*} \quad (43a)$$

is the Fisher information matrix (18),

$$\downarrow X^b = -\frac{\partial x^j}{\partial y_b^*} \frac{\partial^2(\uparrow S)}{\partial x^j \partial x^i} \left(\uparrow L^{ik} \frac{\partial \uparrow \bar{E}}{\partial x^k} + \frac{\partial \uparrow \Xi}{\partial x_i^*} \Big|_{\mathbf{x}^* = \frac{\partial \uparrow S}{\partial \mathbf{x}}} \right) \quad (43b)$$

encodes the detailed evolution projected on the reduced state space, and

$$\|\mathbf{X}\|^2 = -\left(\uparrow L^{ik} \frac{\partial \uparrow \bar{E}}{\partial x^k} + \frac{\partial \uparrow \Xi}{\partial x_i^*} \Big|_{\mathbf{x}^* = \frac{\partial \uparrow S}{\partial \mathbf{x}}} \right) \frac{\partial^2(\uparrow S)}{\partial x^i \partial x^j} \left(\uparrow L^{jk} \frac{\partial \uparrow \bar{E}}{\partial x^k} + \frac{\partial \uparrow \Xi}{\partial x_j^*} \Big|_{\mathbf{x}^* = \frac{\partial \uparrow S}{\partial \mathbf{x}}} \right) \quad (43c)$$

measures the magnitude of the detailed evolution vector field. Note that all \mathbf{g} , $\downarrow \mathbf{X}$, and $\|\mathbf{X}\|^2$ can be functions of \mathbf{y}^* .

In order to find the minimum of the action, we can solve the Euler–Lagrange equations. However, not all geodesics would be thermodynamically relevant as they would lead to exponential blow-ups, as in the toy model in Section 4. Therefore, we would like to find a solution similarly as in that section, using the Onsager-Machlup-like approximation. The Lagrangian is, however, not in the form suitable for that, which is tackled in the next section.

5.2 Onsager-Machlup-like solution

In order to obtain the Onsager-Machlup-like minimizer of action (41), we need to rewrite the Lagrangian in a suitable form, similar to that of (27). Following Kleeman (2015), we carry out a gauge transformation of \mathcal{L} , which does not change the probability distribution,

$$\mathcal{L} + \frac{d\Sigma_e}{dt} - \dot{\mathbf{y}}^* \nabla \Sigma_e - \frac{\partial \Sigma_e}{\partial t} = \frac{1}{2} (\dot{\mathbf{y}}^* - \mathbf{Y}(\Sigma_e, \mathbf{y}^*))^T \mathbf{g} (\dot{\mathbf{y}}^* - \mathbf{Y}(\Sigma_e, \mathbf{y}^*)) + \frac{df}{dt}, \quad (44)$$

where $\Sigma_e(t, \mathbf{y}^*)$ is a gauge function Roncadelli (1992), that will later be identified with the extremal action. The equality is satisfied provided that

$$\mathbf{Y} = \mathbf{g}^{-1}(\nabla \Sigma_e + \downarrow \mathbf{X}) \quad \text{and} \quad \frac{1}{2} \mathbf{Y}^T \mathbf{g} \mathbf{Y} = \frac{1}{2} \|\mathbf{X}\|^2 - \frac{\partial \Sigma_e}{\partial t}, \quad (45)$$

where \mathbf{Y} is the evolution vector field of \mathbf{y}^* we are looking for. The latter condition can also be seen as the Hamilton–Jacobi equation

$$\mathcal{H}(\nabla \Sigma_e, \mathbf{y}^*) + \frac{\partial \Sigma_e}{\partial t} = 0 \quad (46)$$

with the Hamiltonian as the Legendre transform of the Lagrangian (38)

$$\mathcal{H}(\nabla \Sigma_e, \mathbf{y}^*) = (-\mathcal{L}(\mathbf{y}^*, \dot{\mathbf{y}}^*) + \dot{\mathbf{y}}^* \mathbf{p})_{\mathbf{p}=\frac{\partial \mathcal{L}}{\partial \dot{\mathbf{y}}^*}} = \frac{1}{2} (\nabla \Sigma_e + \downarrow \mathbf{X})^T \mathbf{g}^{-1} (\nabla \Sigma_e + \downarrow \mathbf{X}) - \frac{1}{2} \|\mathbf{X}\|^2. \quad (47)$$

The gauge function Σ_e is determined as a solution to the Hamilton–Jacobi equation (46), which means that it represents the extremal action Σ evaluated along the geodesics subject to fixed initial time and state \mathbf{y}_0^* while keeping the final time and state free.

Action $\Delta \Sigma$, which measures the information loss of a particular path, may now be written as

$$\Delta \Sigma = \frac{1}{2} \int_0^T (\dot{\mathbf{y}}^* - \mathbf{Y}(\Sigma_e(t, \mathbf{y}^*), \mathbf{y}^*))^T \mathbf{g} (\dot{\mathbf{y}}^* - \mathbf{Y}(\Sigma_e(t, \mathbf{y}^*), \mathbf{y}^*)) dt + \Sigma_e(T, \mathbf{y}^*(T)) - \Sigma_e(0, \mathbf{y}_0^*). \quad (48)$$

The Onsager-Machlup minimizer of the action is then obtained as in Equation 29, that is by setting the integrand to zero, which is the most probable path,

$$\dot{\mathbf{y}}^* = \mathbf{Y}(\Sigma_e(t, \mathbf{y}^*), \mathbf{y}^*). \quad (49)$$

The action then becomes proportional to the initial value of the gauge function

$$\Delta \Sigma_e = \Sigma_e(T, \mathbf{y}_T^*) - \Sigma_e(0, \mathbf{y}_0^*). \quad (50)$$

Note that later we assume that $\Sigma_e(T, \mathbf{y}_T^*) \approx 0$, as the system approaches the equilibrium. The evolution equation for the reduced state variables \mathbf{y} is obtained from the equation for \mathbf{y}^* ,

$$\begin{aligned}
 \dot{y}^a &= \frac{\partial y^a}{\partial y_b^*} Y^b = \frac{\partial y^a}{\partial y_b^*} g_{bc}^{-1} \left(-\frac{\partial x^j}{\partial y_c^*} \frac{\partial^2 (\uparrow S)}{\partial x^j \partial x^i} \left(\uparrow L^{ik} \frac{\partial \uparrow \bar{E}}{\partial x^k} + \frac{\partial \uparrow \Xi}{\partial x_i^*} \Big|_{\mathbf{x}^* = \frac{\partial \uparrow S}{\partial \mathbf{x}}} \right) + \frac{\partial \Sigma_e}{\partial y_c^*} \right) \\
 &\stackrel{(88)}{=} \frac{\partial y^a}{\partial y_b^*} g_{bc}^{-1} \left(-\left(\frac{\partial \pi^c}{\partial x^i} \Big|_{\mathbf{x}(\mathbf{y}^*)} + \frac{\partial \pi^d}{\partial x^i \partial x^j} \Big|_{\mathbf{x}(\mathbf{y}^*)} \frac{\partial x^j}{\partial y_c^*} y_d^* \right) \left(\uparrow L^{ik} \frac{\partial \pi^e}{\partial x^k} \frac{\partial \downarrow E}{\partial y^e} + \frac{\partial \uparrow \Xi}{\partial x_i^*} \Big|_{\mathbf{x}^* = \frac{\partial \uparrow S}{\partial \mathbf{x}}} \right) + \frac{\partial \Sigma_e}{\partial y_c^*} \right) \\
 &\stackrel{(94)}{=} \left(g^{ab} + y_f^* \frac{\partial^2 \pi^f}{\partial x^m \partial x^n} \Big|_{\mathbf{x}(\mathbf{y}^*)} \frac{\partial x^m}{\partial y_a^*} \frac{\partial x^n}{\partial y_b^*} \right) g_{bc}^{-1} \left(\left(\downarrow L^{ce} \frac{\partial \downarrow E}{\partial y^e} + \frac{\partial \pi^c}{\partial x^i} \Big|_{\mathbf{x}(\mathbf{y}^*)} \frac{\partial \uparrow \Xi}{\partial x_i^*} \Big|_{\mathbf{x}^* = \frac{\partial \uparrow S}{\partial \mathbf{x}}} + \frac{\partial \Sigma_e}{\partial y_c^*} \right) \right. \\
 &\quad \left. + \left(\frac{\partial \pi^d}{\partial x^i \partial x^j} \Big|_{\mathbf{x}(\mathbf{y}^*)} \frac{\partial x^j}{\partial y_c^*} y_d^* \right) \left(\uparrow L^{ik} \frac{\partial \pi^e}{\partial x^k} \frac{\partial \downarrow E}{\partial y^e} + \frac{\partial \uparrow \Xi}{\partial x_i^*} \Big|_{\mathbf{x}^* = \frac{\partial \uparrow S}{\partial \mathbf{x}}} \right) \right).
 \end{aligned}$$

In the case of an affine projection, the second derivatives of π vanish and we obtain that

$$\begin{aligned}
 \dot{y}^a &= \downarrow L^{ab} \frac{\partial \downarrow E}{\partial y^b} + \frac{\partial \pi^a}{\partial x^i} \Big|_{\mathbf{x}(\mathbf{y}^*)} \frac{\partial \uparrow \Xi}{\partial x_i^*} \Big|_{\mathbf{x}^* = \frac{\partial \uparrow S}{\partial \mathbf{x}}(\mathbf{x}(\mathbf{y}^*))} + \frac{\partial \Sigma_e}{\partial y_a^*} \\
 &\stackrel{(88)}{=} \downarrow L^{ab} \frac{\partial \downarrow E}{\partial y^b} + \frac{\partial}{\partial y_a^*} \left(\uparrow \Xi \Big|_{\mathbf{x}^* = \frac{\partial \uparrow S}{\partial \mathbf{x}}(\mathbf{x}(\mathbf{y}^*))} + \Sigma_e \right), \tag{51}
 \end{aligned}$$

which means that the reduced evolution has the GENERIC. The reversible part has again the Hamiltonian form while the dissipation potential has two contributions, one being the detailed dissipation potential evaluated at the MaxEnt image of the reduced conjugate variables, the other being the gauge function.

Note, however, that the procedure works even in the case when the projected Poisson bivector is not automatically independent of the detailed variables, in which case the Jacobi identity may be violated. Moreover, the reduction does not automatically result in the degeneracy conditions required in the usual GENERIC framework Kraaij et al. (2018).

Also, it is not automatically guaranteed that the Onsager-Casimir reciprocal relations are satisfied by the reduced dissipative dynamics, as the principle of detailed balance is not imposed a priori. Finally, the obtained dissipation potential $\Sigma_e(t, \mathbf{y}^*)$ can in general be a function of time, which is also different from the usual GENERIC framework, where the dissipation potential depends on the reduced state variables \mathbf{y} and the conjugate state variables \mathbf{y}^* , but not explicitly on time. The Hamilton-Jacobi equation solved here might be connected with the Hamilton-Jacobi equation for the dissipation potential that is needed for the fully geometric formulation of the GENERIC framework Esen et al. (2022a), and the underlying Onsager-Machlup principle seems related to the Rate-GENERIC system Esen et al. (2022b). These features will be further investigated in the future, in connection with the principle of large deviations Kraaij et al. (2018).

In order to close the evolution equation, we need to determine the extremal action Σ_e by solving the Hamilton-Jacobi equation (46). In particular, we expect that as $t \rightarrow \infty$, the extremal action will go to zero, which means that the system

will reach equilibrium,

$$\Sigma_e(\infty, \mathbf{y}^*(\infty)) = 0. \quad (52)$$

Although the Hamilton–Jacobi equation is often difficult to solve, the next chapter shows how to do it in the case of the Kac–Zwanzig model.

Near the thermodynamic equilibrium, where the matrices in the Lagrangian \mathcal{L} can be considered constant, the Lagrangian itself is a convex function of the paths. Therefore, the resulting dissipation potential Σ_e is also convex near the equilibrium, which guarantees the second law of thermodynamics (growth of entropy $\downarrow S$), see B.

In summary, the lack-of-fit reduction leads to a GENERIC evolution equation (51) for the reduced state variables \mathbf{y} with a dissipation potential that is the sum of the detailed dissipation potential and the extremal action Σ_e . The lack-of-fit, measured by the action, thus serves as a dissipation potential for the reduced evolution. In particular, purely Hamiltonian systems can be reduced to a dissipative dynamics, and the method does not require any fitting parameters. In the following Section, we show how to bring back some elements of the unresolved detailed dynamics in the form of fluctuations of the reduced dynamics.

5.3 Stochasticity

When a system is described by a Langevin equation, probability of a path can be expressed as the exponential of an action Ventsel’ and Freidlin (1970), and the minimum of the action then gives the most probable path.

Here, following Kleeman (2015), we go in the opposite direction. The path-integral formulation (37) gives probabilities of individual paths, from which we can reconstruct the corresponding Langevin equation for the reduced state variables \mathbf{y}^*

$$d\mathbf{y}^* = \mathbf{Y}dt + \mathbf{\Pi}d\mathbf{W} \implies d\mathbf{y} = (\downarrow\mathbf{X} + \nabla\Sigma_e(\mathbf{y}^*, T, t)) dt + \mathbf{g}\mathbf{\Pi}d\mathbf{W} \quad (53)$$

where

$$\mathbf{\Pi}^T\mathbf{\Pi} = \frac{1}{\Delta t}\mathbf{g}^{-1} \quad (54)$$

and $d\mathbf{W}$ is a Wiener process. Although the reconstruction of the noise is not unique in general, when the metric is diagonal and we assume that the noise is also a diagonal matrix, the noise can be determined from the metric, as in the following Section on the Kac–Zwanzig model.

6 Kac–Zwanzig example

Let us now illustrate the general lack-of-fit reduction on the Kac–Zwanzig model Ford et al. (1965); Zwanzig (2001); Stuart and Warren (1999a). The Kac–Zwanzig model is a classical Hamiltonian model of friction that exhibits effectively irreversible evolution of a large particle interacting with many small particles. The reduction of the Kac–Zwanzig model can be calculated analytically for some specific distributions of the frequencies of the small particles (connected via springs to the large particle) Ariel and Vanden-Eijnden (2008); Kupferman et al. (2011). However, there is no general

analytical theory available for any distribution of the frequencies, that would not eventually rely on the measurement of the Green-Kubo relations and fluctuations of the detailed dynamics Kubo (1957); Zwanzig (2001); Grabert (2006); Español et al. (2019). The lack-of-fit reduction provides an alternative way to obtain the reduced evolution for a general distribution of the spring constants.

6.1 The Kac–Zwanzig model

The Kac–Zwanzig model is one of the classical Hamiltonian models of friction Ford et al. (1965). It consists of a large particle of mass M moving in a potential $V(\mathbf{Q})$ and interacting with N small particles of mass m_i ($i = 1, \dots, N$) via harmonic springs. Under certain conditions, the large particle exhibits effectively irreversible evolution, despite the overall system being reversible.

It can be shown that the evolution of the large particle is governed by a stochastic differential equation, when the number of small particles goes to infinity Stuart and Warren (1999a). Here, we use the Kac–Zwanzig model to illustrate a new general theory of reduction in non-equilibrium thermodynamics.

The Hamiltonian function of the system is

$$H = \frac{\mathbf{P}^2}{2M} + V(\mathbf{Q}) + \sum_{i=1}^N \left[\frac{\mathbf{p}_i^2}{2m_i} + \frac{\gamma}{2N} (\mathbf{q}_i - \mathbf{Q})^2 \right], \quad (55)$$

where \mathbf{Q} and \mathbf{P} are the position and momentum of the large particle, \mathbf{q}_i and \mathbf{p}_i are the positions and momenta of the small particles, and γ/N is the spring constant. The equations of motion implied by this Hamiltonian are

$$\begin{aligned} \dot{\mathbf{Q}} &= \frac{\partial H}{\partial \mathbf{P}} & \dot{\mathbf{q}}_i &= \frac{\partial H}{\partial \mathbf{p}_i} \\ \dot{\mathbf{P}} &= -\frac{\partial H}{\partial \mathbf{Q}} & \dot{\mathbf{p}}_i &= -\frac{\partial H}{\partial \mathbf{q}_i}. \end{aligned} \quad (56a)$$

Before going to the lack-of-fit reduction itself, let us recall the reduction of the Kac–Zwanzig model based on the projection operator method Zwanzig (2001); Öttinger (2005).

6.2 Reduction by the Projection Operator Method

Using the projection operators technique for the Hamiltonian equations, the position and momentum of the large particle can be shown to satisfy the following integro-differential equations Zwanzig (2001):

$$\dot{\mathbf{Q}} = \frac{\mathbf{P}}{M}, \quad \dot{\mathbf{P}} = -\frac{\partial V}{\partial \mathbf{Q}} - \int_0^t \Gamma(s) \frac{\mathbf{P}(t-s)}{M} ds + \mathbf{F}(t) \quad (57)$$

$$M\ddot{\mathbf{Q}} + \frac{\partial V}{\partial \mathbf{Q}} + \int_0^t \Gamma(s) \dot{\mathbf{Q}}(t-s) ds = \mathbf{F}(t) \quad (58)$$

with the memory kernel $\Gamma(s)$ and the force $\mathbf{F}(t)$:

$$\begin{aligned}\Gamma(t) &= -\Theta(t) \frac{\gamma}{N} \sum_j \cos(\omega_j t) = -\Theta(t) \frac{2}{\pi} \int_0^\infty d\omega' \frac{J(\omega')}{\omega'} \cos(\omega' t), \\ \mathbf{F}(t) &= \frac{\gamma}{N} \sum_j \left[(\mathbf{q}_j(0) - \mathbf{Q}(0)) \cos(\omega_j t) + \frac{\mathbf{p}_j(0)}{\omega_j m_j} \sin(\omega_j t) \right],\end{aligned}$$

where the spectral density is defined as

$$J(\omega) = \frac{\pi}{2} \frac{\gamma}{N} \sum_j \omega_j \delta(\omega - \omega_j).$$

In the Markovian approximation, where the large particle is governed by a couple of ordinary differential equations, the memory kernel is assumed to be approximated by a delta function,

$$\Gamma(t) \approx \delta(t) \underbrace{\int_0^\infty \Gamma(s) ds}_{\stackrel{def}{=} \gamma_{theor}}. \quad (59)$$

Assuming, moreover, that the force in Equation (58) is negligible (taking the average over the ensemble of small particles), the effective equation of motion of the large particle simplifies to

$$M\ddot{\mathbf{Q}} + \frac{\partial V}{\partial \mathbf{Q}} + \gamma_{theor} \dot{\mathbf{Q}} = 0, \quad (60)$$

where γ_{theor} is the theoretical friction coefficient. This equation describes the motion of the large particle within potential field $V(\mathbf{Q})$ and with the damping coefficient γ_{theor} .

In order to calculate the friction coefficient, we assume that N is large enough so that the spectral density $J(\omega)$ can be approximated by a continuous function. We shall study two particular cases:

1. The distribution of ω_j^2 is uniform between $(0, \omega_{max}^2)$. The spectral density and the friction coefficient are given by

$$J(\omega) = \frac{\pi}{2} \frac{2\gamma}{\omega_{max}^2} \omega^2 \quad 0 \leq \omega \leq \omega_{max}, \quad (61a)$$

$$\Gamma(t) = -\Theta(t) \frac{2\gamma}{\omega_{max}^2} \left[\frac{\omega_{max} \sin(\omega_{max} t)}{t} + \frac{\cos(\omega_{max} t) - 1}{t^2} \right], \quad (61b)$$

$$\gamma_{theor} = 0. \quad (61c)$$

2. The distribution of ω_j is uniform between $(0, \omega_{max})$:

$$J(\omega) = \frac{\pi}{2} \frac{\gamma}{\omega_{max}} \omega \quad 0 \leq \omega \leq \omega_{max}, \quad (62a)$$

$$\Gamma(t) = -\Theta(t) \frac{\gamma}{\omega_{max}} \frac{\sin(\omega_{max}t)}{t}, \quad (62b)$$

$$\gamma_{theor} = \gamma \int_0^{\infty} \frac{\sin(\omega_{max}t)}{\omega_{max}t} dt = \frac{\gamma\pi}{2\omega_{max}}. \quad (62c)$$

It can be seen that even the sole presence of the friction term in the Markovian limit depends on the spectral density of the small particles. While Equation (60) will serve as a benchmark for the numerical simulations, we will show cases when the effective evolution is damped despite the absence of the friction term in the Markovian limit. The lack-of-fit reduction, on the other hand, will be able to reproduce friction even in the absence of the friction term in the Markovian limit.

6.3 Lack-of-fit reduction

Let us now apply the lack-of-fit reduction to the Kac–Zwanzig model with the quadratic potential $V(\mathbf{Q}) = \frac{1}{2}\alpha\mathbf{Q}^2$. Although the results will be similar as in Mladá et al. (2024), here we use a different formulation of the reduction method, presented in Section 5, and we add a stochastic generalization.

6.3.1 Formulation of the Lack-of-fit Lagrangian

The first step is to choose the reduced state variables. While the detailed variables are given by the distribution function of all particles $f(\mathbf{Q}, \mathbf{P}, \mathbf{q}_1, \mathbf{p}_1, \dots, \mathbf{q}_N, \mathbf{p}_N)$, which follows the Liouville equation, the reduced state variables are then chosen as the following averages,

$$\bar{\mathbf{Q}} = \frac{1}{N!} \int \int \dots \int f(\mathbf{Q}, \mathbf{P}, \mathbf{q}_1, \mathbf{p}_1, \dots, \mathbf{q}_N, \mathbf{p}_N) \mathbf{Q} d\mathbf{Q} d\mathbf{P} d\mathbf{q}_1 d\mathbf{p}_1 \dots d\mathbf{q}_N d\mathbf{p}_N, \quad (63a)$$

$$\bar{\mathbf{P}} = \frac{1}{N!} \int \int \dots \int f(\mathbf{Q}, \mathbf{P}, \mathbf{q}_1, \mathbf{p}_1, \dots, \mathbf{q}_N, \mathbf{p}_N) \mathbf{P} d\mathbf{Q} d\mathbf{P} d\mathbf{q}_1 d\mathbf{p}_1 \dots d\mathbf{q}_N d\mathbf{p}_N, \quad (63b)$$

$$\bar{s} = \frac{1}{N!} \int \int \dots \int f(\mathbf{Q}, \mathbf{P}, \mathbf{q}_1, \mathbf{p}_1, \dots, \mathbf{q}_N, \mathbf{p}_N) \left(\frac{1}{N} \sum_{i=1}^N \mathbf{q}_i - \mathbf{Q} \right) d\mathbf{Q} d\mathbf{P} d\mathbf{q}_1 d\mathbf{p}_1 \dots d\mathbf{q}_N d\mathbf{p}_N, \quad (63c)$$

$$\bar{e} = \frac{1}{N!} \int \int \dots \int f(\mathbf{Q}, \mathbf{P}, \mathbf{q}_1, \mathbf{p}_1, \dots, \mathbf{q}_N, \mathbf{p}_N) H(\mathbf{Q}, \mathbf{P}, \mathbf{q}_1, \mathbf{p}_1, \dots, \mathbf{q}_N, \mathbf{p}_N) d\mathbf{Q} d\mathbf{P} d\mathbf{q}_1 d\mathbf{p}_1 \dots d\mathbf{q}_N d\mathbf{p}_N, \quad (63d)$$

which represent the average position of the big particle, its average momentum, the average distance of the small particles from the big particle, and the average energy of the system, respectively. The Lagrangian is then, see Mladá et al. (2024) for details,

$$\mathcal{L} = \frac{1}{2}(\dot{\mathbf{y}}^*)^T \mathbb{C} \dot{\mathbf{y}}^* + (\dot{\mathbf{y}}^*)^T \mathbb{B}^T \mathbf{y}^* + \frac{1}{2} \mathbf{y}^{*T} \mathbb{A} \mathbf{y}^*, \quad (64)$$

where $\mathbf{y}^{*T} \equiv (Q^*, P^*, s^*, E^*)$ are the conjugate reduced variables. In the notation of Section 5, Lagrangian (64) gives

$$\|\mathbf{X}\|^2 = \mathbf{y}^* \mathbb{A} \mathbf{y}^{*T}; \quad \mathbf{g} = \mathbb{C}; \quad \downarrow \mathbf{X} = -\mathbb{B}^T \mathbf{y}^* \quad (65)$$

with matrices

$$\mathbb{A} = \frac{1}{E^*} \begin{pmatrix} \frac{1}{M} & 0 & -\frac{1}{M} & 0 \\ 0 & \alpha + \gamma & 0 & 0 \\ -\frac{1}{M} & 0 & \frac{1}{M} + \frac{\overline{\omega^2}}{\gamma} & 0 \\ 0 & 0 & 0 & 0 \end{pmatrix}, \quad \mathbb{B} = \frac{1}{E^*} \begin{pmatrix} 0 & 1 & 0 & -\frac{P^*}{E^*} \\ -1 & 0 & 1 & \frac{Q^* - s^*}{E^*} \\ 0 & -1 & 0 & \frac{P^*}{E^*} \\ 0 & 0 & 0 & 0 \end{pmatrix}, \quad (66)$$

and

$$\mathbb{C} = \frac{1}{E^*} \begin{pmatrix} \frac{1}{\alpha} & 0 & 0 & -\frac{Q^*}{E^* \alpha} \\ 0 & M & 0 & -\frac{MP^*}{E^*} \\ 0 & 0 & \frac{1}{\gamma} & -\frac{s^*}{E^* \gamma} \\ -\frac{Q^*}{E^* \alpha} & -\frac{MP^*}{E^*} & -\frac{s^*}{E^* \gamma} & \frac{k_B E^* (N+1) + 2\Sigma}{(E^*)^2} \end{pmatrix}, \quad (67)$$

where $\overline{\omega^2} = \frac{1}{N} \sum_{i=1}^N \omega_i^2$ is the average of the squared frequencies of the small particles and E^* is the inverse temperature (derivative of entropy with respect to energy). In order to close the reduced evolution equations, we need to determine the extremal action Σ_e by solving the Hamilton–Jacobi equation (46).

6.3.2 The Hamilton–Jacobi equation

Hamilton–Jacobi equation (46) becomes

$$-\frac{\partial \Sigma_e}{\partial t} = \frac{1}{2} \left[-\mathbf{y}^{*T} \mathbb{A} \mathbf{y}^* + \left(\frac{\partial \Sigma_e}{\partial \mathbf{y}^*} - \mathbf{y}^{*T} \mathbb{B} \right) \mathbb{C}^{-1} \left(\frac{\partial \Sigma_e}{\partial \mathbf{y}^*} - \mathbb{B}^T \mathbf{y}^* \right) \right] \quad (68)$$

with the condition $\Sigma_e(\mathbf{y}^*(T), T) = 0$. Using an Ansatz $\Sigma_e(\mathbf{y}^*, t) = -\frac{1}{2E^*} \mathbf{y}^{*T} \mathbb{M}(t) \mathbf{y}^*$, the solution is found using the Riccati matrix equation

$$-\frac{1}{(E^*)^2} \mathbb{M} \mathbb{C}^{-1} \mathbb{M} - \frac{1}{E^*} \mathbb{M} \mathbb{C}^{-1} \mathbb{B}^T - \frac{1}{E^*} \mathbb{B} \mathbb{C}^{-1} \mathbb{M} + \mathbb{A} - \mathbb{B} \mathbb{C}^{-1} \mathbb{B}^T = -\frac{1}{E^*} \dot{\mathbb{M}} \quad (69)$$

with $\mathbb{M}(T) = 0$. The Riccati equation has both stable and unstable solutions, but only the stable solution is physically relevant as it corresponds to a positive definite dissipation. The stable solution can be written as

$$\mathbb{M}(t) = \left(\mathbb{W}_{21} - \mathbb{W}_{22} e^{-\Lambda(T-t)} \mathbb{W}_{22}^{-1} \mathbb{W}_{21} e^{-\Lambda(T-t)} \right) \left(\mathbb{W}_{11} - \mathbb{W}_{12} e^{-\Lambda(T-t)} \mathbb{W}_{22}^{-1} \mathbb{W}_{21} e^{-\Lambda(T-t)} \right)^{-1}, \quad (70)$$

with \mathbb{W}_{ij} determined from

$$\mathbb{H} = \begin{pmatrix} -\hat{\mathbb{C}}^{-1} \hat{\mathbb{B}}^T & -\hat{\mathbb{C}}^{-1} \\ \hat{\mathbb{B}} \hat{\mathbb{C}}^{-1} \hat{\mathbb{B}}^T - \hat{\mathbb{A}} & \hat{\mathbb{B}} \hat{\mathbb{C}}^{-1} \end{pmatrix} \equiv \begin{pmatrix} \mathbb{W}_{11} & \mathbb{W}_{12} \\ \mathbb{W}_{21} & \mathbb{W}_{22} \end{pmatrix} \begin{pmatrix} \Lambda & 0 \\ 0 & -\Lambda \end{pmatrix} \begin{pmatrix} \mathbb{W}_{11} & \mathbb{W}_{12} \\ \mathbb{W}_{21} & \mathbb{W}_{22} \end{pmatrix}^{-1},$$

see Kučera (1973). The existence of stable solution is conditioned by the existence of positive diagonal matrix $\text{Re}(\Lambda)$.

6.3.3 The reduced dynamics

Within the interval $(0, T)$, the conjugate reduced variables \mathbf{y}^* then evolve according to

$$\dot{\mathbf{y}}^* = \mathbf{g}^{-1} (\nabla \Sigma_e(\mathbf{y}^*, t) + \downarrow \mathbf{X}) = \mathbb{C}^{-1} \left(\frac{1}{E^*} \mathbb{M}(t) - \mathbb{B}^T \right) \mathbf{y}^*, \quad (71)$$

as follows from Equation (49).

For the evolution of \mathbf{y} , we need to obtain $\frac{\partial \mathbf{y}(\mathbf{y}^*)}{\partial \mathbf{y}^*}$, which corresponds to $-\mathbb{C}$,

$$\dot{\mathbf{y}} = \left(\mathbb{B}^T - \frac{1}{E^*} \mathbb{M}(t) \right) \mathbb{C}^{-1} \mathbf{y}. \quad (72)$$

The concrete form of the matrix $\mathbb{M}(t)$ will be determined later by asymptotic analysis and numerically.

The action $\Delta \Sigma_e$, calculated for the evolution (71), is

$$\Delta \Sigma_e = -\Sigma_e(\mathbf{y}_0^*, 0) = \frac{1}{2E^*} \mathbf{y}_0^{*T} \mathbb{M}(0; T) \mathbf{y}_0^*, \quad (73)$$

and it indicates the lack-of-fit between the reduced and detailed evolution vector fields. For initial conditions $(y_0^*)^T = (Q_0, 0, 0, 0)$, action (73) reduces to

$$\Delta \Sigma_e = \frac{(Q_0^*)^2}{2E^*} \mathbb{M}_{11} = \frac{\alpha^2 \bar{Q}_0^2}{2T} \mathbb{M}_{11}, \quad (74)$$

since $Q^* = -\alpha \bar{Q} E^*$ and $E^* = 1/T$.

6.3.4 Asymptotic solution of the Riccati equation

We employ asymptotic methods to solve the stationary case of the Riccati equation (69) in the large-time region, when \mathbb{M} is approximately constant. First, we rescale the matrices into the following non-dimensional form (omitting the common prefactor of all the terms in the Riccati equation)

$$\tilde{\mathbb{A}} = \begin{pmatrix} 1 & 0 & -1 \\ 0 & 1+b & 0 \\ -1 & 0 & 1+\rho \end{pmatrix}, \quad \tilde{\mathbb{B}} = \begin{pmatrix} 0 & 1 & 0 \\ -1 & 0 & 1 \\ 0 & -1 & 0 \end{pmatrix}, \quad \tilde{\mathbb{C}} = \begin{pmatrix} b^{-1} & 0 & 0 \\ 0 & 1 & 0 \\ 0 & 0 & 1 \end{pmatrix}, \quad (75)$$

where we introduced $\rho = b \frac{\omega^2}{\alpha M}$ with $0 < b = \frac{\alpha}{\gamma}$. Note that we have omitted the fourth row and column of the Riccati equation for simplicity. For asymptotic calculations, we consider the physically relevant scenario of a large frequency ratio squared, that is, $1 \ll \rho$ while $b = \mathcal{O}(1)$.

The algebraic Riccati equation can be rewritten as the following set of quadratic equations for the sought matrix $\tilde{\mathbb{M}}$:

$$0 = -\tilde{m}_{12}(2 + \tilde{m}_{12}) - \tilde{m}_{13}^2 - \tilde{m}_{11}^2 b, \quad (76a)$$

$$0 = -(1 + \tilde{m}_{12})\tilde{m}_{22} - \tilde{m}_{13}(1 + \tilde{m}_{23}) + \tilde{m}_{11}(1 - \tilde{m}_{12})b, \quad (76b)$$

$$0 = \tilde{m}_{12} - \tilde{m}_{23}(1 + \tilde{m}_{12}) - \tilde{m}_{13}(\tilde{m}_{11}b + \tilde{m}_{33}), \quad (76c)$$

$$0 = -\tilde{m}_{22}^2 - \tilde{m}_{23}(2 + \tilde{m}_{23}) + (2 - \tilde{m}_{12})\tilde{m}_{12}b, \quad (76d)$$

$$0 = \tilde{m}_{22}(1 - \tilde{m}_{23}) - (1 + \tilde{m}_{23})\tilde{m}_{33} + (1 - \tilde{m}_{12})\tilde{m}_{13}b, \quad (76e)$$

$$0 = (2 - \tilde{m}_{23})\tilde{m}_{23} - \tilde{m}_{33}^2 - \tilde{m}_{13}^2 b + \rho, \quad (76f)$$

where we employed the required symmetry of the dissipative potential, noting that the dimensional dissipation matrix then follows from

$$\mathbb{M} = \begin{pmatrix} \rho \tilde{m}_{11} & \tilde{m}_{12} & \rho \tilde{m}_{13} \\ \tilde{m}_{12} & \rho^{-1} \tilde{m}_{22} & \tilde{m}_{23} \\ \rho \tilde{m}_{13} & \tilde{m}_{23} & \rho \tilde{m}_{33} \end{pmatrix}.$$

To find an asymptotic solution of the set of equations (76a) for $\rho \gg 1$, it is crucial to find the correct asymptotic order of all the six unknowns \tilde{m}_{ij} by dominant balance. It can be shown that the following choice of asymptotic orders yields a balance

$$\begin{aligned} \tilde{m}_{11} &= \mathcal{O}(1), \tilde{m}_{12} = \mathcal{O}(1), \tilde{m}_{13} = \mathcal{O}(\rho^{-1/2}), \\ \tilde{m}_{22} &= \mathcal{O}(1), \tilde{m}_{23} = \mathcal{O}(1), \tilde{m}_{33} = \mathcal{O}(\rho^{1/2}), \end{aligned}$$

from where it is easy to find the (eight) leading order solutions. They are for the dimensional problem

$$\begin{aligned} m_{11} &= (M\alpha)^{-1/2} z_1 \left(\left(\frac{1}{b} - 4 - 8b \right) + 8z_2 \sqrt{b(1+b)} \right)^{1/2} = (M\alpha)^{-1/2} z_1 \sqrt{\frac{1}{b} + 4m_{12}}, \\ m_{12} &= -1 - 2b + 2z_2 \sqrt{b(1+b)}, \\ m_{13} &= (M\alpha)^{-1/2} z_3 \left(z_2(1+4b) - b\sqrt{b(1+b)} \right)^{1/2} \rho^{-1/2}, \\ m_{22} &= (M\alpha)^{1/2} z_1 z_2 \sqrt{b(1+b)} \left(\left(\frac{1}{b} - 4 - 8b \right) + 8z_2 \sqrt{b(1+b)} \right)^{1/2} = (M\alpha) z_2 \sqrt{b(1+b)} m_{11}, \\ m_{23} &= -1, \\ m_{33} &= -(M\alpha)^{-1/2} z_2 z_3 \rho^{1/2}, \end{aligned}$$

where z_j are undetermined, $z_j \in \{-1, 1\}$ for all j , that is, there are 8 solutions.

Finally, as the dissipative matrix has to be positive semidefinite, we require $z_1 = +1 = z_2$, $z_3 = -1$ entailing the unique positive definite dissipative matrix \mathbb{M} :

$$m_{11} = (M\alpha)^{-1/2} \left(\left(\frac{1}{b} - 4 - 8b \right) + 8\sqrt{b(1+b)} \right)^{1/2}, \quad (77a)$$

$$m_{12} = -1 - 2b + 2\sqrt{b(1+b)}, \quad (77b)$$

$$m_{13} = -(M\alpha)^{-1/2} \left(z_2(1+4b) - b\sqrt{b(1+b)} \right)^{1/2} \rho^{-1/2}, \quad (77c)$$

$$m_{22} = (M\alpha)^{1/2} \sqrt{b(1+b)} \left(\left(\frac{1}{b} - 4 - 8b \right) + z_2 8\sqrt{b(1+b)} \right)^{1/2}, \quad (77d)$$

$$m_{23} = -1, \quad (77e)$$

$$m_{33} = (M\alpha)^{-1/2} \rho^{1/2}. \quad (77f)$$

For example, with $M = 1099$, $\alpha = 1$, $b = 1$, $\rho = 37$ we get the following asymptotic estimate:

$$\mathbb{M} = \begin{pmatrix} 0.0168952 & -0.171573 & 0.0198139 \\ & 26.2589 & -1 \\ & & 0.0301648 \end{pmatrix},$$

while the numerical solution reads:

$$\mathbb{M} = \begin{pmatrix} 0.0166733 & -0.1696847 & 0.002148 \\ & 25.1330519 & -0.76117 \\ & & 0.179169 \end{pmatrix}.$$

The asymptotic solution is thus in good agreement with the numerical solution of Riccati equation.

6.3.5 Stochasticity

The Langevin equation for the reduced variables (53) is given by

$$\Pi = \frac{1}{\sqrt{\Delta t}} \begin{pmatrix} \frac{1}{\sqrt{\alpha}} & 0 & 0 \\ 0 & \sqrt{M} & 0 \\ 0 & 0 & \frac{1}{\sqrt{\gamma}} \end{pmatrix}. \quad (78)$$

Parameter Δt is calculated as $\Delta t = \frac{dt_{min}^2}{\Omega}$, where $dt_{min} = \frac{2\pi}{\omega_{max}}$ is the smallest typical time of the small particles, ω_{max} is the highest frequency of the small particles, and Ω is the frequency of the big particle (frequency of a harmonic oscillator). Figure 3 compares the deterministic and stochastic results.

6.3.6 Numerical results

In this section, we present the results of the numerical simulations of the Kac–Zwanzig model, similar to those in Stuart and Warren (1999b); Hald and Kupferman (2002); Mladá et al. (2024). The detailed results are obtained by directly integrating the equations of motion (56) for the detailed variables. The reduced equations of motion are obtained by integrating equations (51) together with the Riccati equation (69) in the deterministic case, and the Langevin equation (53) in the stochastic case.

To increase the precision, the simulations are performed for the reduced state variables \mathbf{Q} , \mathbf{P} , and s with extra state variables Ψ_{mi} or Ψ_{Σ} ,

$$\Psi_{mi} = \sum_i \frac{p_i}{Nm_i} \quad \text{or} \quad \Psi_{\Sigma} = \frac{\sum_i p_i}{N \sum_j m_j}, \quad (79)$$

see Mladá et al. (2024) for more details on the calculations. Figure 3 shows the trajectories for various initial conditions. It compares several variants of the lack-of-fit reduction with the projection operator method and the direct numerical simulation of the Kac–Zwanzig model. First, the non-stationary reduction with reduced variables \mathbf{Q} , \mathbf{P} , and s , which too much shows damping, is present. The non-stationarity means that we let the dissipation potential $\Sigma_e(t, \mathbf{y}^*)$ depend explicitly on time and we solve the corresponding Riccati equation numerically. The Ψ_{mi} method (with state variables \mathbf{Q} , \mathbf{P} , s , Ψ_{mi}) is a bit less overdamped, and we also show its stochastic extension. The closest agreement between

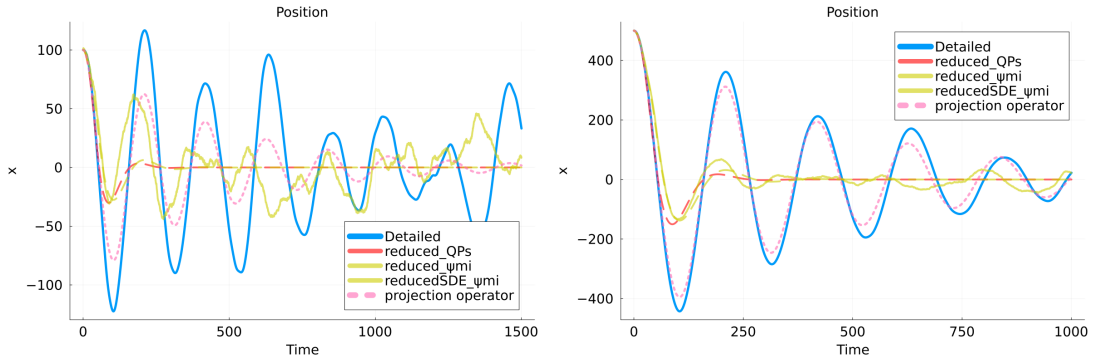


Figure 3: Comparison of the deterministic and stochastic results for different choices of the extra state variables (79) and two different initial positions of the big particle (left: $x_0 = 100$, right: $x_0 = 500$). The deterministic results are presented in the stationary and non-stationary cases, the former corresponding to the stationary solution of the Hamilton–Jacobi (or Riccati) equation, the latter to the non-stationary, where the action $\Sigma_e(t, \mathbf{y}^*)$ depends also explicitly on time. Parameters of the simulation were $N = 10000$, $\gamma = 1.0$, $\alpha = 1.0$, ω_i sampled from uniformly from the interval $(\sqrt{1.0E-05}, \sqrt{1.0E-01})$, and M was set equal to the total mass of the small particles.

the detailed and reduced dynamics is obtained by the projection operator method. However, for other choices of the distribution ω_i , the projection operator method could even lead to zero dissipation, as in Figure 4, so we focus on the lack-of-fit methods.

From the lack-of-fit methods, that with Ψ_{mi} gives the best results among the lack-of-fit reductions, especially in the non-stationary case, when the dissipation potential Σ_e depends explicitly on time. When Ψ_{Σ} is used, instead of Ψ_{mi} , the deviation with respect to the detailed simulation is a bit higher. The simplest set of state variables, \mathbf{Q} , \mathbf{P} , and s gives

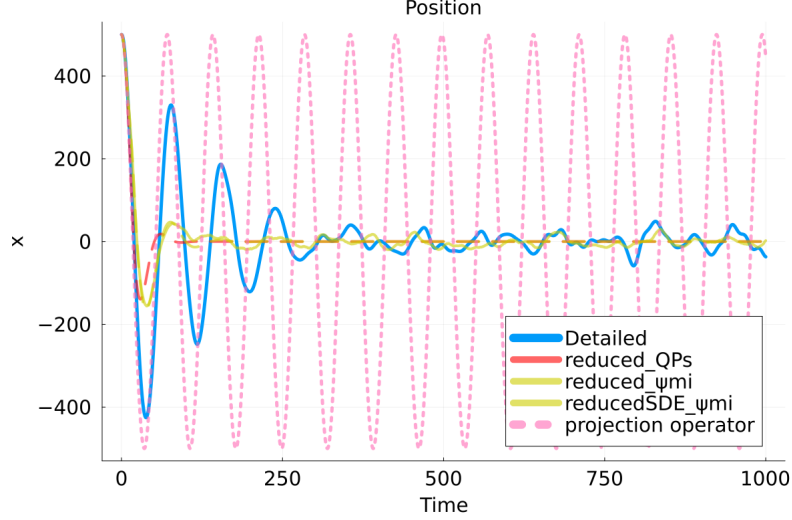


Figure 4: Comparison of the deterministic and stochastic results for the initial condition $Q_0 = 1000$ and ω_i sampled from the uniform distribution ω_i^2 between 10^{-5} and 10^{-1} . The projection operator method gives zero dissipation. The only difference between this simulation and that in Figure 3 is the distribution of ω_i .

the worst results, as expected. The stochastic version is able to reconstruct to some extent the equilibrium fluctuations of the big particle, caused by the motion of the cloud of small particles.

Section 6.3.7 shows that the KL divergence between the distributions of the detailed and reduced dynamics is the lowest for Ψ_{mi} , followed by Ψ_Σ , and the highest for the simplest set of reduced state variables, which explains the order of precision of those choices Mladá et al. (2024).

6.3.7 KL Divergence

Let us suppose that we have two choices of reduced variables \mathbf{y} , \mathbf{z} such that their functional derivatives $\frac{\delta \mathbf{y}}{\delta f}$, $\frac{\delta \mathbf{z}}{\delta f}$ are not functions of reduced variables. Their maximum entropy distributions $\tilde{f}(x; \mathbf{y}^*)$, $\tilde{f}(x; \mathbf{z}^*)$ then are of the form:

$$\tilde{f}(x; \mathbf{y}^*) = \frac{1}{\mathcal{Z}(\mathbf{y}^*)} \exp\left(-\frac{1}{k_B} \frac{\delta \mathbf{y}}{\delta f} \cdot \mathbf{y}^*\right),$$

with $\mathcal{Z}(\mathbf{y}^*)$ the normalization constant. Their Kullback–Leibler divergence is given as:

$$D_{\text{KL}}(\tilde{f}(x; \mathbf{y}^*) \parallel \tilde{f}(x; \mathbf{z}^*)) = \int d\Omega(x) \tilde{f}(x; \mathbf{y}^*) \log\left(\frac{\mathcal{Z}(\mathbf{z}^*)}{\mathcal{Z}(\mathbf{y}^*)}\right) \frac{1}{k_B} \left(\frac{\delta \mathbf{z}}{\delta f} \cdot \mathbf{z}^* - \frac{\delta \mathbf{y}}{\delta f} \cdot \mathbf{y}^*\right).$$

Final formulas are given in Table 1, detailed calculations in F. For our parameters of the Kac–Zwanzig model, the lowest KL divergence is obtained for the Ψ_{mi} distribution, followed by Ψ_Σ , and the highest for the simplest set of reduced variables \mathbf{Q} , \mathbf{P} , and s . This is in agreement with the numerical results Mladá et al. (2024).

$D_{\text{KL}}(\Downarrow \rightarrow)$	f_{QP}	f_s	f_{m_i}	f_Σ
f_{QP}	0	0	0	0
f_s	$\frac{1}{2} \left(\frac{\gamma \overline{s^2}}{k_B T} \right)^2$	0	0	0
f_{m_i}	$\frac{1}{2} \left(\frac{\gamma \overline{s^2} + N \overline{\psi_{m_i}^2} / \frac{1}{m}}{k_B T} \right)^2$	$\frac{1}{2} \left(\frac{N \overline{\psi_{m_i}^2}}{k_B T \frac{1}{m}} \right)^2$	0	$\frac{\Delta_a \Delta_c \overline{\psi_{m_i}}}{2 \frac{1}{m}} \left(\frac{N}{k_B T} \right)^2$
f_Σ	$\frac{1}{2} \left(\frac{\gamma \overline{s^2} + N \overline{m} N^2 \overline{\psi_\Sigma^2}}{k_B T} \right)^2$	$\frac{1}{2} \left(\frac{N \overline{m} N^2 \overline{\psi_\Sigma^2}}{k_B T} \right)^2$	$\frac{\Delta_a \Delta_b N \overline{\psi_\Sigma}}{2} \left(\frac{N}{k_B T} \right)^2$	0

Table 1: Kullback–Leibler divergence of several distributions. $\Delta_a = \frac{\overline{\psi_{m_i}^2}}{\frac{1}{m}} - N^2 \overline{m} \overline{\psi_\Sigma^2}$; $\Delta_b = \frac{\overline{\psi_{m_i}}}{\frac{1}{m}} - N \overline{m} \overline{\psi_\Sigma}$; $\Delta_c = \overline{\psi_{m_i}} - N \overline{\psi_\Sigma}$

7 Conclusion

In this paper, we have reformulated the lack-of-fit reduction method in the context of path integrals, generalizing the approach of Kleeman Kleeman (2015). To do so, we had to generalize the concept of Kullback–Leibler divergence and Fisher information matrix to arbitrary entropies. The resulting lack-of-fit reduction method then leads to reduced dynamics of the GENERIC form, where a dissipation potential emerges encoding the discrepancy between the detailed (unresolved) evolution and the reduced evolution equations. The method is then tested on the Kac–Zwanzig model, showing a qualitative agreement with the numerical results (with no fitting parameters). In particular, even purely Hamiltonian dynamics can be reduced to a system with fewer degrees of freedom and dissipation then emerges on the reduced level of description. Dissipation can be thus seen as a consequence of the lack of knowledge about the detailed dynamics.

The generalized Kullback–Leibler divergence can be used even in the case when the entropy is not in the Shannon–Boltzmann–Gibbs form, for instance with the Tsallis–Havrda–Charvát entropy.

Three levels of the lack-of-fit reduction are calculated in the context of the Kac–Zwanzig model, differing in the choice of the reduced state variables. The best agreement between the reduced and detailed dynamics is obtained for the set of reduced state variables that has the lowest KL divergence between the distributions of the detailed and reduced dynamics.

Finally, the path-integral formulation also provides a way to introduce stochasticity into the reduced dynamics. The Langevin equation is then derived from the path-integral Lagrangian. Fluctuations can be then seen also as a consequence of the lack of knowledge about the detailed dynamics.

In the future, we would like to focus on problems with boundary conditions, on a large-deviation generalization of the method, and on applications to systems in continuum thermodynamics.

Acknowledgements

Authors were supported by the Czech Science Foundation (GACR) under project 23-05736S. MP is a member of the Nečas Center for Mathematical Modeling. KM is supported by Charles University, project GA UK No. 414225.

A MaxEnt KL divergence with Tsallis-Havrda-Charvát entropy

In this section, we show how the generalized MaxEnt KL divergence (16) works in the case of the Tsallis-Havrda-Charvát entropy Tsallis (1988); Havrda and Charvát (1967),

$$\uparrow S_q^{\text{Tsallis}}(\mathbf{p}) = - \sum_i p_i \log_q p_i = - \sum_i p_i \frac{p_i^{1-q} - 1}{1-q}, \quad (80)$$

where q is the entropic index, parametrizing a family of entropies, and $\log_q(x) = \frac{x^{1-q} - 1}{1-q}$. This entropy is a powerful generalization of the Boltzmann-Gibbs-Shannon entropy (recovered for $q = 1$), as its MaxEnt distributions fit a large class of physical phenomena Tsallis (2023).

We assume that the detailed variables are given by a distribution with probabilities p_i while the reduced variables are given by probabilities q_i . First, we have to calculate the reducing potential,

$$\downarrow \tilde{S}^*(\mathbf{p}, \mathbf{q}^*) = \frac{1}{1-q} \sum_i p_i (p_i^{1-q} - 1) + \sum_i q_i^* p_i. \quad (81)$$

The potential has a minimum at $p_i(\mathbf{q}^*) = \left(\frac{1-(1-q)q_i^*}{2-q} \right)^{1/(1-q)}$, and when evaluated at this minimum, it gives the lower conjugate entropy

$$\downarrow S^*(\mathbf{q}^*) = \sum_i \left(\frac{(q-1)q_i^* + 1}{2-q} \right)^{\frac{2-q}{1-q}}. \quad (82)$$

The consequent Legendre transformation $q_i = \frac{\partial \downarrow S^*}{\partial q_i^*}$ gives a relation $q_i^* = \frac{(2-q)q_i^{1-q} - 1}{q-1}$.

The MaxEnt KL divergence then becomes

$$D_{KL}^M L(\mathbf{p}||\mathbf{q}) = \sum_i p_i (\log_q p_i - \log_q q_i) + (1-q) \sum_i (q_i - p_i) \log_q q_i. \quad (83)$$

In the case when $q = 1$, this KL divergence simplifies to the standard KL divergence for Shannon entropy. Formula (83) is, however, different from the usual KL divergence for the Tsallis entropy Furuichi et al. (2004),

$$D_{KL}^M(\mathbf{p}||\mathbf{q}) \neq - \sum_i p_i \log_q \frac{p_i}{q_i}. \quad (84)$$

For $q = 1$, the two divergences coincide and simplify to the standard KL divergence for Shannon entropy. As the generalized KL divergence is only a by-product of this manuscript, we leave further analysis for future work.

B Convexity of the dissipation potential

In this section, we show how the convexity of the dissipation potential Σ_e follows from the convexity of the Lagrangian \mathcal{L} .

Consider two geodesics $\mathbf{y}^{*1}(t)$ and $\mathbf{y}^{*2}(t)$ that have the same starting point \mathbf{y}_0^* but different end points \mathbf{y}_T^{*1} and \mathbf{y}_T^{*2} at time T . Then, let us define the interpolated path $\mathbf{y}^{*\lambda}(t) = (1 - \lambda)\mathbf{y}^{*1}(t) + \lambda\mathbf{y}^{*2}(t)$ for $\lambda \in [0, 1]$, which has the same start point as the two geodesics while having the interpolated end point $\mathbf{y}_T^{*\lambda} = (1 - \lambda)\mathbf{y}_T^{*1} + \lambda\mathbf{y}_T^{*2}$.

The action along the interpolated path is given by

$$\Sigma(\mathbf{y}_T^{*\lambda}, T) = \int_0^T \mathcal{L}(\mathbf{y}^{*\lambda}(t), \dot{\mathbf{y}}^{*\lambda}(t)) dt. \quad (85)$$

From the convexity of the Lagrangian, expressed by the Jensen's inequality, we have that

$$\Sigma(\mathbf{y}_T^{*\lambda}, T) \leq (1 - \lambda)\Sigma_e(\mathbf{y}_T^{*1}, T) + \lambda\Sigma_e(\mathbf{y}_T^{*2}, T), \quad (86)$$

where Σ_e is on the right-hand side, where the action is evaluated along the geodesics $\mathbf{y}^{*1}(t)$ and $\mathbf{y}^{*2}(t)$, respectively.

When we take the minimum of the action on the left-hand side with respect to paths with the endpoint $\mathbf{y}_T^{*\lambda}$, we obtain

$$\Sigma_e((1 - \lambda)\mathbf{y}_T^{*1} + \lambda\mathbf{y}_T^{*2}, T) \leq (1 - \lambda)\Sigma_e(\mathbf{y}_T^{*1}, T) + \lambda\Sigma_e(\mathbf{y}_T^{*2}, T), \quad (87)$$

which means that the dissipation potential Σ_e is convex in the end point \mathbf{y}_T^* .

C Details on the MaxEnt calculation

Let us recall a few rather technical but useful relations Pavelka et al. (2020a). Taking another derivative of the MaxEnt equation (8), we obtain that

$$\frac{\partial^2 \uparrow S}{\partial x^i \partial x^j} \Big|_{\mathbf{x}(\mathbf{y}^*)} \frac{\partial x^j}{\partial y_b^*} = \frac{\partial \pi^b}{\partial x^i} \Big|_{\mathbf{x}(\mathbf{y}^*)} + \frac{\partial^2 \pi^a}{\partial x^i \partial x^j} \Big|_{\mathbf{x}(\mathbf{y}^*)} \frac{\partial x^j}{\partial y_b^*} y_a^*. \quad (88)$$

In the case of affine mapping π , the second term vanishes.

Another useful formula shows how the Hessian of the reduced conjugate entropy relates to the Hessian of the detailed entropy. The first derivative of the definition of the reduced conjugate entropy (9) gives

$$\frac{\partial \downarrow S^*}{\partial y_a^*} = -\frac{\partial \uparrow S}{\partial x^i} \frac{\partial x^i}{\partial y_a^*} + \pi^a + \frac{\partial \pi^b}{\partial x^i} \Big|_{\mathbf{x}(\mathbf{y}^*)} \frac{\partial x^i}{\partial y_a^*} y_b^*. \quad (89)$$

The second derivative is then

$$\begin{aligned} \frac{\partial^2 \downarrow S^*}{\partial y_a^* \partial y_b^*} = & -\frac{\partial^2 \uparrow S}{\partial x^i \partial x^j} \Big|_{\mathbf{x}(\mathbf{y}^*)} \frac{\partial x^i}{\partial y_a^*} \frac{\partial x^j}{\partial y_b^*} - \frac{\partial \uparrow S}{\partial x^i} \Big|_{\mathbf{x}(\mathbf{y}^*)} \frac{\partial^2 x^i}{\partial y_a^* \partial y_b^*} + \frac{\partial \pi^a}{\partial x^i} \Big|_{\mathbf{x}(\mathbf{y}^*)} \frac{\partial x^i}{\partial y_b^*} \\ & + \frac{\partial^2 \pi^c}{\partial x^i \partial x^j} \Big|_{\mathbf{x}(\mathbf{y}^*)} \frac{\partial x^i}{\partial y_a^*} \frac{\partial x^j}{\partial y_b^*} y_c^* + \frac{\partial \pi^c}{\partial x^i} \Big|_{\mathbf{x}(\mathbf{y}^*)} \frac{\partial^2 x^i}{\partial y_a^* \partial y_b^*} y_c^* + \frac{\partial \pi^b}{\partial x^i} \Big|_{\mathbf{x}(\mathbf{y}^*)} \frac{\partial x^i}{\partial y_a^*}. \end{aligned} \quad (90)$$

In order to simplify the right hand side of this expression, we take derivative of the equality

$$\pi(\mathbf{x}(\mathbf{y}^*(\mathbf{y}))) = \mathbf{y}, \quad (91)$$

which tells us that the projection π of the MaxEnt mapping is the identity. After the differentiation, we obtain

$$\left. \frac{\partial \pi^a}{\partial x^i} \right|_{\mathbf{x}(\mathbf{y}^*(\mathbf{y}))} \frac{\partial x^i}{\partial y_a^*} \frac{\partial y_a^*}{\partial y^b} = \delta_b^a, \quad (92)$$

which means that

$$\left. \frac{\partial \pi^a}{\partial x^i} \right|_{\mathbf{x}(\mathbf{y}^*)} \frac{\partial x^i}{\partial y_b^*} = \frac{\partial y^a}{\partial y_b^*} = \frac{\partial^2 \downarrow S^*}{\partial y_a^* \partial y_b^*}. \quad (93)$$

Equality (90) can be simplified to

$$-g^{ab} = \frac{\partial^2 \downarrow S^*}{\partial y_a^* \partial y_b^*} + y_c^* \left. \frac{\partial^2 \pi^c}{\partial x^i \partial x^j} \right|_{\mathbf{x}(\mathbf{y}^*)} \frac{\partial x^i}{\partial y_a^*} \frac{\partial x^j}{\partial y_b^*}, \quad (94)$$

where g^{ab} is the Fisher information matrix (43a).

D Details on solving the Hamilton–Jacobi equation

In this section, we show the details of solving the Hamilton–Jacobi equation (26). With the quadratic Ansatz

$$S(u, t) = k(t)u^2 + b(t)u + c(t)$$

the derivatives of the action become

$$\frac{\partial S}{\partial u} = 2k(t)u + b(t)$$

$$\frac{\partial S}{\partial t} = \dot{k}(t)u^2 + \dot{b}(t)u + \dot{c}(t)$$

or

$$\dot{k}(t)u^2 + \dot{b}(t)u + \dot{c}(t) = -\frac{1}{2} \left[(2k(t)u + b(t))^2 - \kappa^2 u^2 \right].$$

This last equation can be solved as

$$\dot{k}(t) = \frac{-4k^2(t) + \kappa^2}{2} \Rightarrow k(t) = \frac{\kappa}{2} \tanh(\kappa(t + C_1)),$$

$$\dot{b}(t) = -2k(t) \cdot b(t) \Rightarrow b(t) = \frac{C_2}{\cosh(\kappa(t + C_1))},$$

$$\dot{c}(t) = -\frac{b^2(t)}{2} \Rightarrow c(t) = C_3 - \frac{C_2^2 \sinh(\kappa t)}{2\kappa \cosh(2\kappa C_1) \cosh(\kappa(t + C_1))},$$

which leads to the action

$$S(u, t) = \frac{\kappa}{2} \tanh(\kappa(t + C_1))u^2 + \frac{C_2}{\cosh(\kappa(t + C_1))}u - \frac{C_2^2 \sinh(\kappa t)}{2\kappa \cosh(2\kappa C_1) \cosh(\kappa(t + C_1))} + C_3. \quad (95)$$

From the first equation of the H-J theory:

$$\dot{u} = \kappa u \tanh(\kappa(t + C_1)) + \frac{C_2}{\cosh(\kappa(t + C_1))}, \quad (96)$$

solution of which is

$$u(t) = \frac{C_2}{\kappa} \sinh(\kappa(t + C_1)) + \tilde{C} \cosh(\kappa(t + C_1)), \quad (97)$$

in other words, geodesics.

To compare the result with the action (25), we need to relate u_T, T, t_0 and $u(0) = u_0$ to the constants C_1, C_2 , and C_3 . As constant C_1 only shifts the time, we can set $C_1 = 0$, thus fixing the initial time $t_0 = 0$. The other two constants are then found by relating $u(0) = u_0$ and $u(T) = u_T$. We arrive at $S(u, t)$ in the form

$$S = \frac{\kappa}{2} \coth(\kappa T) (u_T^2 + u_0^2) - \kappa \frac{u_0 u_T}{\sinh(\kappa T)}, \quad (98)$$

which is the same solution as obtained by solving the Euler–Lagrange equation (25).

E Alternative trajectories of the toy model

Instead of solving the whole Euler–Lagrange equation or the Hamilton–Jacobi equation, which eventually lead to both damped and exploding solutions and second-order differential equations, we shall look for approximate solutions that only show the damped solutions. This is because the exploding solutions would be thermodynamically irrelevant and exponentially less probable in the context of large deviations Mielke et al. (2016); Kraaij et al. (2018).

E.1 Quasistatic approximation

One possibility to eliminate the exponentially growing parts of the action is to use the following quasistatic approximation. The momentum in the Hamilton–Jacobi equation is associated with the gradient of the action, $p = \frac{\partial S}{\partial u}$. Therefore, in this quasistatic approximation one can assume that the momentum is small as in Kleeman (2015). This leads to the equation

$$\frac{\partial S_e}{\partial u_T} = 0 \implies u_T = \frac{u_0}{\cosh \kappa T}, \quad (99)$$

solution of which is

$$S_e(T, u_T(\text{ex.})) = \frac{\kappa u_0^2}{2} \tanh \kappa T. \quad (100)$$

However, this is not the only approach to thermodynamically relevant actions.

E.2 Stepest-descent approximation

One might, for instance, search for trajectories that always go along the steepest descent in the action, that is along

$$\nabla_z S_e \left(\frac{\partial S_e}{\partial T}, \frac{\partial S_e}{\partial u_T} \right), \quad z = (T, u_T), \quad dz = -\alpha \nabla_z S_e. \quad (101)$$

The motion can be then described by the following equations,

$$dT = -\alpha \frac{\partial S}{\partial T}, \quad du_T = -\alpha \frac{\partial S}{\partial u_T}, \quad \frac{du_T}{dT} = \frac{\frac{\partial S}{\partial u_T}}{\frac{\partial S}{\partial T}}, \quad (102)$$

and with the derivatives

$$\frac{\partial S}{\partial T} = \frac{u_0^2 + u_T^2 + 2u_0u_T \cosh(T)}{2 \sinh(T)^2}, \quad \frac{\partial S}{\partial u_T} = \frac{\cosh(T)}{\sinh(T)}u_T - \frac{u_0}{\sinh(T)}$$

we obtain the approximate solution

$$\frac{du_T}{dT} = 2 \sinh(T) \frac{\cosh(T)u_T - u_0}{u_0^2 + u_T^2 + 2u_0u_T \cosh(T)}, \quad (103)$$

which always goes along the steepest descent of the action. The solution of this equation is plotted in Figures 5, 6, and 7 together with the quasistatic solution (99) and the Onsager-Machlup-like solution (see below). In the Figures, the steepest-descent solution is actually a result of a backward integration of Equation (102), which is stable, in contrast to the direct forward integration of that equation.

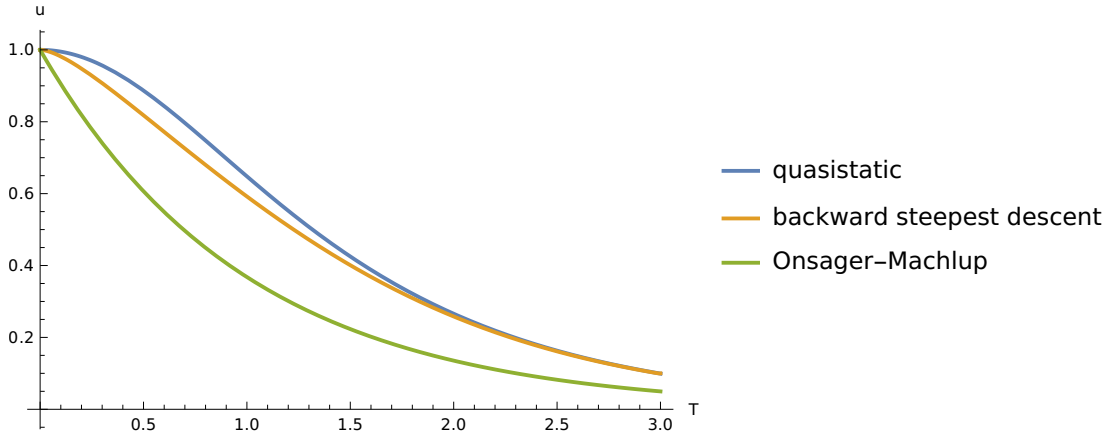


Figure 5: Plot of the quasistatic solution of (99) (blue), the steepest descent solution (103) (orange), and the Onsager-Machlup (OM) solution (29) (green), all for $\kappa = 1$ and $u_0 = 1$. The OM solution is the most damped of all.

E.3 Comparison of the approximate solutions

Which of the approximate solutions is the best from the thermodynamic point of view? The quasistatic solution gives the lowest action neither in the beginning nor at the end of the time interval, see Figure 8. Moreover, it is similar to the direct projection of on a slow submanifold Turkington (2013) where irreversibility does not appear out of the reversible dynamics by reduction. In other words, if no dissipation is present before the reduction (here approximation), no dissipation would be present in the reduced dynamics.

The steepest descent solution always goes in the direction of the lowest action. Initially, it has a lower action than the OM solution, but eventually, as it approaches the equilibrium and converges to the OM solution, it acquires higher action. Moreover, to obtain a stable solution, Equation (102) has to be solved backwards in time, starting from a final value of u_T and time T .

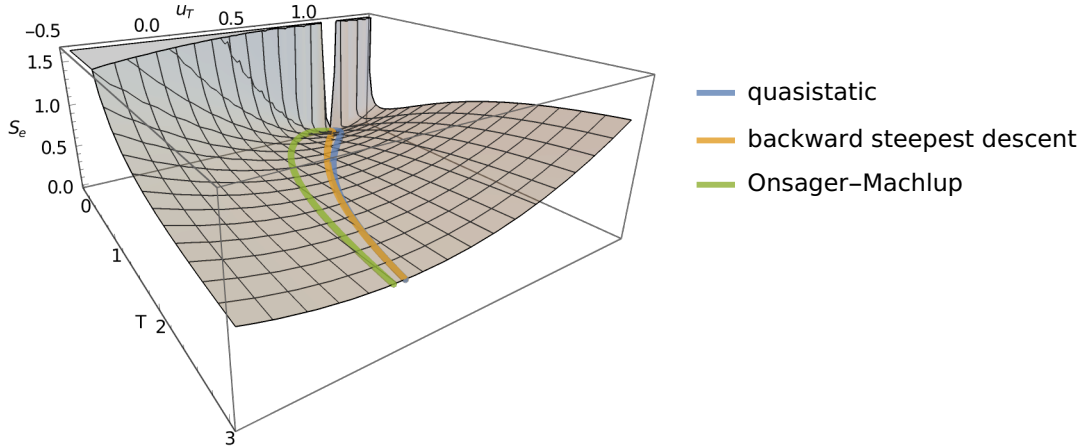


Figure 6: Plot of the function $S_e(T, u_T)$ (25) and several trajectories: Plot of the quasistatic solution of (99) (blue), the steepest descent solution (103) (orange), and the Onsager-Machlup (OM) solution (29) (green), all for $\kappa = 1$ and $u_0 = 1$. The backward-mode quasistatic solutions goes along the bottom of the S_e valley.

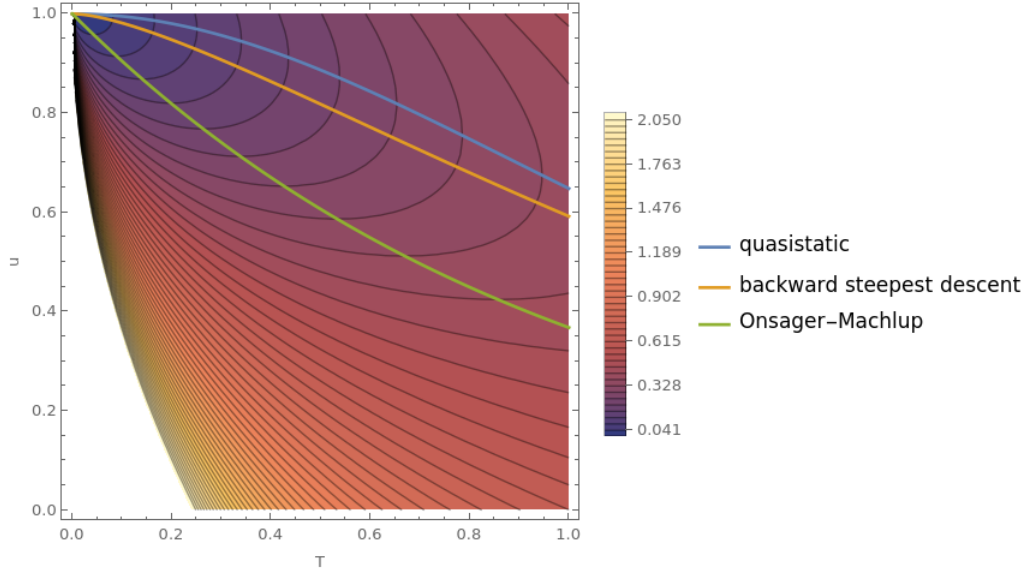


Figure 7: Plot of the function $S_e(T, u_T)$ (25) (contours) and several trajectories: Plot of the quasistatic solution of (99) (blue), the steepest descent solution (103) (orange), and the Onsager-Machlup (OM) solution (29) (green), all for $\kappa = 1$ and $u_0 = 1$. The OM solution is the most damped of all. The backward-mode steepest descent solution is perpendicular to the contours of $S_e(T, u_T)$.

The OM solution, being a true geodesic, always gives the lowest action for any trajectory ending at u_T and T . In particular, as all the approximate solutions tend to the equilibrium as $T \rightarrow \infty$, the action of the OM solution tends

to the lowest value. Moreover, the OM solution best reflects the probabilistic interpretation of non-equilibrium thermodynamics, where the action represents the probability of a path, and only those paths with zero action (up to some boundary-dependent terms) are relevant Mielke et al. (2016).

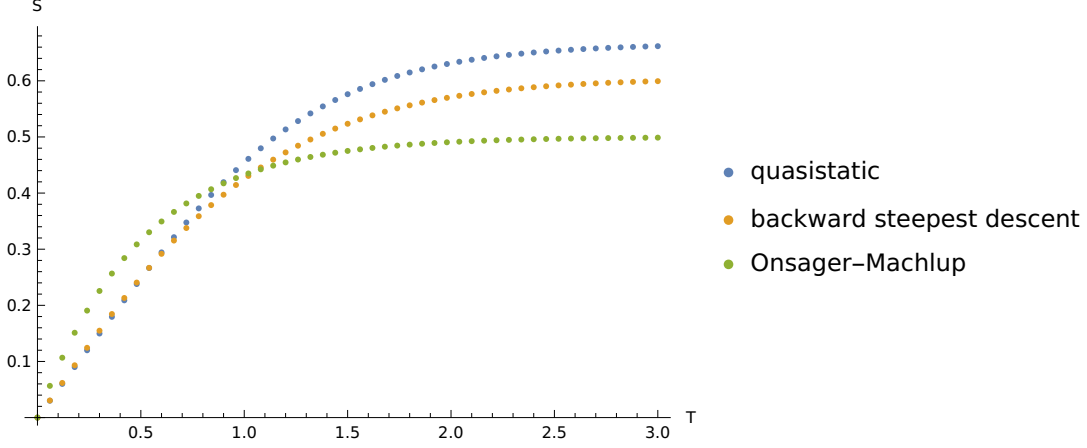


Figure 8: Plot of action S along the approximate solutions: the quasistatic solution (99) (blue), the steepest descent solution (103) (orange), and the Onsager-Machlup (OM) solution (29) (green), all for $\kappa = 1$ and $u_0 = 1$.

F Calculation of the Kullback–Leibler divergence

With the choices of variables given in Table 1, each result has the form:

$$\log \left(\frac{\mathcal{Z}(\mathbf{z}^*)}{\mathcal{Z}(\mathbf{y}^*)} \right) \frac{1}{k_B} \left(\left\langle \frac{\delta \mathbf{z}}{\delta f} \right\rangle_{\mathbf{y}} \cdot \mathbf{z}^* - \left\langle \frac{\delta \mathbf{y}}{\delta f} \right\rangle_{\mathbf{y}} \cdot \mathbf{y}^* \right),$$

with $\langle \cdot \rangle_{\mathbf{y}}$ denoting the mean value with respect to the distribution $\tilde{f}(x; \mathbf{y}^*)$ where \mathcal{Z} is a number dependent on the parameters of the model, e.g. masses of particles etc.,

$$\mathcal{Z}(\mathbf{y}^*) = \mathcal{Z} \exp \left(-\frac{T\Sigma(\mathbf{y}^*)}{2k_B} \right) \equiv \mathcal{Z} \exp \left(\frac{1}{2k_B} \left\langle \frac{\delta \mathbf{y}}{\delta f} \right\rangle_{\mathbf{y}} \cdot \mathbf{y}^* \right).$$

This allows us to write

$$D_{\text{KL}}(\tilde{f}(x; \mathbf{y}^*) \parallel \tilde{f}(x; \mathbf{z}^*)) = \frac{1}{2k_B^2} \left(\left\langle \frac{\delta \mathbf{z}}{\delta f} \right\rangle_{\mathbf{y}} \cdot \mathbf{z}^* - \left\langle \frac{\delta \mathbf{y}}{\delta f} \right\rangle_{\mathbf{y}} \cdot \mathbf{y}^* \right) \left(\left\langle \frac{\delta \mathbf{z}}{\delta f} \right\rangle_{\mathbf{z}} \cdot \mathbf{z}^* - \left\langle \frac{\delta \mathbf{y}}{\delta f} \right\rangle_{\mathbf{y}} \cdot \mathbf{y}^* \right).$$

The mean values $\langle s \rangle_{QP} = \langle \psi_{\Sigma} \rangle_{QP} = \langle \psi_{mi} \rangle_{QP} = \langle \psi_{\Sigma} \rangle_{QP_s} = \langle \psi_{mi} \rangle_{QP_s} = 0$, since in both models the mean value of p_i is 0 for all particles and the positions of small particles in the QP model have as the mean value the position of the large particle Q . Note that $s = \sum_i (q_i - Q)/N$, $\psi_{\Sigma} = \sum_i p_i / (N \sum_j m_j)$, and $\psi_{mi} = \sum_i p_i / (N m_i)$. This leaves only the calculation of $\langle \psi_{mi} \rangle_{\Sigma}$, $\langle \psi_{\Sigma} \rangle_{mi}$, which after a few tedious operations leads to the mean values

$$\langle \psi_{mi} \rangle_{\Sigma} \psi_{mi}^* = \langle \psi_{\Sigma} \rangle_{mi} \psi_{\Sigma}^* = -\frac{T}{N \sum_j m_j} \psi_{\Sigma}^* \psi_{mi}^*.$$

References

- Ariel, G. and Vanden-Eijnden, E. (2008). A strong limit theorem in the Kac–Zwanzig model. *Nonlinearity*, 22(1):145.
- Beris, A. and Edwards, B. (1994). *Thermodynamics of Flowing Systems*. Oxford Univ. Press, Oxford, UK.
- Dzyaloshinskii, I. E. and Volovick, G. E. (1980). Poisson brackets in condense matter physics. *Annals of Physics*, 125(1):67–97.
- Esen, O., Pavelka, M., and Grmela, M. (2022a). On the role of geometry in statistical mechanics and thermodynamics I: Geometric perspective. *J. Math. Phys.*, 63(122902).
- Esen, O., Pavelka, M., and Grmela, M. (2022b). On the role of geometry in statistical mechanics and thermodynamics II: Thermodynamic perspective. *J. Math. Phys.*, 63(123305).
- Español, P., de la Torre, J. A., and Duque-Zumajo, D. (2019). Solution to the plateau problem in the green-kubo formula. *Phys. Rev. E*, 99:022126.
- Fecko, M. (2006). *Differential Geometry and Lie Groups for Physicists*. Cambridge University Press.
- Fisher, R. A. and Russell, E. J. (1922). On the mathematical foundations of theoretical statistics. *Philosophical Transactions of the Royal Society of London. Series A, Containing Papers of a Mathematical or Physical Character*, 222(594-604):309–368.
- Ford, G. W., Kac, M., and Mazur, P. (1965). Statistical mechanics of assemblies of coupled oscillators. *Journal of Mathematical Physics*, 6:504–515.
- Furuichi, S., Yanagi, K., and Kuriyama, K. (2004). Fundamental properties of tsallis relative entropy. *Journal of Mathematical Physics*, 45(12):4868–4877.
- Gelfand, I. and Fomin, S. (2012). *Calculus of Variations*. Dover Books on Mathematics. Dover Publications.
- Gorban, A. and Karlin, I. (2005). *Invariant Manifolds for Physical and Chemical Kinetics*. Lecture Notes in Physics. Springer.
- Gorban, A. N., Karlin, I. V., Öttinger, H. C., and Tatarinova, L. L. (2001). Ehrenfest’s argument extended to a formalism of nonequilibrium thermodynamics. *Physical Review E*, 63(066124).
- Grabert, H. (2006). *Projection Operator Techniques in Nonequilibrium Statistical Mechanics*. Springer Tracts in Modern Physics. Springer Berlin Heidelberg.
- Grmela, M. (1984). Particle and bracket formulations of kinetic equations. *Contemporary Mathematics*, 28:125–132.
- Grmela, M. (2012). Fluctuations in extended mass-action-law dynamics. *Physica D Nonlinear Phenomena*, 241:976–986.
- Grmela, M. (2024). Thermodynamics and rate thermodynamics. *J Stat Phys*, 191(75).
- Grmela, M., Klika, V., and Pavelka, M. (2015). Reductions and extensions in mesoscopic dynamics. *Phys. Rev. E*, 92(032111).

- Grmela, M. and Öttinger, H. C. (1997). Dynamics and thermodynamics of complex fluids. I. Development of a general formalism. *Phys. Rev. E*, 56:6620–6632.
- Hald, O. H. and Kupferman, R. (2002). Asymptotic and numerical analyses for mechanical models of heat baths. *Journal of Statistical Physics*, 106(5):1121–1184.
- Havrda, J. and Charvát, F. (1967). Quantification method of classification processes. concept of structural α -entropy. *Kybernetika*, 3(1):30–35.
- Jaynes, E. T. (1967). *Delaware Seminar in the Foundation of Physics*, M. Bunge ed., chapter Foundations of probability theory and statistical mechanics. Springer New York.
- Jizba, P. and Korbel, J. (2019). Maximum entropy principle in statistical inference: Case for non-shannonian entropies. *Phys. Rev. Lett.*, 122:120601.
- Karlin, I. V., Tatarinova, L. L., Gorban, A. N., and Öttinger, H. C. (2003). Irreversibility in the short memory approximation. *Physica A: Statistical Mechanics and its Applications*, 327(3-4):399–424.
- Kleeman, R. (2015). A path integral formalism for non-equilibrium hamiltonian statistical systems. *Journal of Statistical Physics*, 158(6):1271–1297.
- Kraaij, R., Lazarescu, A., Maes, C., and Peletier, M. (2018). Deriving generic from a generalized fluctuation symmetry. *Journal of Statistical Physics*, 170(3):492–508.
- Kubo, R. (1957). Statistical-mechanical theory of irreversible processes. I. General theory and simple applications to magnetic and conduction problems. *Journal of the Physical Society of Japan*, 12(6):570–586.
- Kučera, V. (1973). A review of the matrix Riccati equation. *Kybernetika*, 09(1):(42)–61.
- Kullback, S. and Leibler, R. A. (1951). On information and sufficiency. *Annals of Mathematical Statistics*, 22(1):79–86.
- Kupferman, R., Stuart, A., Terry, J., and Tupper, P. (2011). Long-term behavior of large mechanical systems with random initial data. *Stochastics and Dynamics*, 02.
- Leadbetter, T., Purohit, P. K., and Reina, C. (2023). A statistical mechanics framework for constructing nonequilibrium thermodynamic models. *PNAS Nexus*, 2(12):pgad417.
- Maack, J. and Turkington, B. (2018). Reduced models of point vortex systems. *Entropy*, 20(12).
- Mielke, A., Peletier, M. A., and Renger, D. R. M. (2014). On the relation between gradient flows and the large-deviation principle, with applications to Markov chains and diffusion. *Potential Analysis*, 41(4):1293–1327.
- Mielke, A., Peletier, M. A., and Zimmer, J. (2025). Deriving a generic system from a hamiltonian system.
- Mielke, A., Renger, D. R. M., and Peletier, M. A. (2016). A generalization of Onsager’s reciprocity relations to gradient flows with nonlinear mobility. *Journal of Non-equilibrium Thermodynamics*, 41(2).
- Mladá, K., Šípka, M., and Pavelka, M. (2024). Lack-of-fit reduction in non-equilibrium thermodynamics applied to the kac–zwanzig model. *Journal of Non-Equilibrium Thermodynamics*, 49(2):181–194.

- Montefusco, A., Peletier, M. A., and Öttinger, H. C. (2021). A framework of nonequilibrium statistical mechanics. ii. coarse-graining. *Journal of Non-Equilibrium Thermodynamics*, 46(1):15–33.
- Mori, H. (1965). Transport, collective motion, and Brownian motion. *Progress of Theoretical Physics*, 33(3):423–455.
- Morrison, P. J. (1984). Bracket formulation for irreversible classical fields. *Physics Letters A*, 100(8):423–427.
- Onsager, L. and Machlup, S. (1953). Fluctuations and irreversible processes. *Physical Review*, 91(6):1505–1512.
- Öttinger, H. (2005). *Beyond Equilibrium Thermodynamics*. Wiley, New York.
- Öttinger, H. C. and Grmela, M. (1997). Dynamics and thermodynamics of complex fluids. II. Illustrations of a general formalism. *Phys. Rev. E*, 56:6633–6655.
- Öttinger, H. C., Peletier, M. A., and Montefusco, A. (2021). A framework of nonequilibrium statistical mechanics. i. role and types of fluctuations. *Journal of Non-Equilibrium Thermodynamics*, 46(1):1–13.
- Pavelka, M., Klika, V., and Grmela, M. (2018). *Multiscale Thermo-Dynamics*. de Gruyter, Berlin.
- Pavelka, M., Klika, V., and Grmela, M. (2019). Ehrenfest regularization of Hamiltonian systems. *Physica D: Nonlinear phenomena*, 399:193–210.
- Pavelka, M., Klika, V., and Grmela, M. (2020a). Generalization of the dynamical lack-of-fit reduction. *Journal of Statistical Physics*, 181(1):19–52.
- Pavelka, M., Peshkov, I., and Klika, V. (2020b). On Hamiltonian continuum mechanics. *Physica D: Nonlinear phenomena*, 408(132510).
- Rao, C. R. (1992). *Information and the Accuracy Attainable in the Estimation of Statistical Parameters*, pages 235–247. Springer New York, New York, NY.
- Roncadelli, M. (1992). New path integral representation of the quantum mechanical propagator. *Journal of Physics A: Mathematical and General*, 25(16):L997.
- Shannon, C. E. (1948). A mathematical theory of communication. *Bell System Technical Journal*, 27:379–423,623–656.
- Stuart, A. M. and Warren, J. O. (1999a). Analysis and experiments for a computational model of a heat bath. *Journal of Statistical Physics*, 97(3):687–723.
- Stuart, A. M. and Warren, J. O. (1999b). Analysis and experiments for a computational model of a heat bath. *Journal of Statistical Physics*, 97(3):687–723.
- Thalabard, S. and Turkington, B. (2017). Optimal response to non-equilibrium disturbances under truncated burgers–hopf dynamics. *Journal of Physics A: Mathematical and Theoretical*, 50(17):175502.
- Tsallis, C. (1988). Possible generalization of Boltzmann-Gibbs statistics. *Journal of Statistical Physics*, 52(1-2):479–487.
- Tsallis, C. (2023). *Introduction to Nonextensive Statistical Mechanics: Approaching a Complex World*. Springer Cham.

- Turkington, B. (2013). An optimization principle for deriving nonequilibrium statistical models of hamiltonian dynamics. *J Stat Phys*, 152:569–597.
- Turkington, B., Chen, Q.-Y., and Thalabard, S. (2016). Coarse-graining two-dimensional turbulence via dynamical optimization. *Nonlinearity*, 29(10):2961–2989.
- Ventsel', A. D. and Freidlin, M. I. (1970). On small random perturbations of dynamical systems. *Russian Mathematical Surveys*, 25(1):1.
- Zwanzig, R. (2001). *Nonequilibrium Statistical Mechanics*. Oxford University Press, USA.